HHS Public Access

Author manuscript

Mol Cell Neurosci. Author manuscript; available in PMC 2024 June 01.

Published in final edited form as:

Mol Cell Neurosci. 2023 June ; 125: 103847. doi:10.1016/j.mcn.2023.103847.

Chemogenetic inhibition of TrkB signalling reduces phrenic motor neuron survival and size

Matthew J. Fogarty,

Debanjali Dasgupta,

Obaid U. Khurram,

Gary C. Sieck

Department of Physiology and Biomedical Engineering Mayo Clinic, Rochester, MN, 55905, USA.

Abstract

Brain derived neurotrophic factor (BDNF) signalling through its high-affinity tropomyosin receptor kinase B (TrkB) is known to have potent effects on motor neuron survival and morphology during development and in neurodegenerative diseases. Here, we employed a novel 1NMPP1 sensitive *TrkB*^{F616} rat model to evaluate the effect of 14 days inhibition of TrkB signalling on phrenic motor neurons (PhMNs). Adult female and male *TrkB*^{F616} rats were divided into 1NMPP1 or vehicle treated groups. Three days prior to treatment, PhMNs in both groups were initially labeled via intrapleural injection of Alexa-Fluor-647 cholera toxin B (CTB). After 11 days of treatment, retrograde axonal uptake/transport was assessed by secondary labeling of PhMNs by intrapleural injection of Alexa-Fluor-488 CTB. After 14 days of treatment, the spinal cord was excised 100 μm thick spinal sections containing PhMNs were imaged using two-channel confocal microscopy. TrkB inhibition reduced the total number of PhMNs by ~16%, reduced the mean PhMN somal surface areas by ~25%, impaired CTB uptake 2.5-fold and reduced the estimated PhMN dendritic surface area by ~38%. We conclude that inhibition of TrkB signalling alone in adult *TrkB*^{F616} rats is sufficient to lead to PhMN loss, morphological degeneration and deficits in retrograde axonal uptake/transport.

Keywords

retrograde transport; phrenic motor neurons; neurotrophins; neural plasticity

*Correspondence: Gary C. Sieck, Department of Physiology & Biomedical Engineering, Mayo Clinic, 200 1st St SW, Rochester, MN 55905, sieck.gary@mayo.edu.

Author Contribution: MF and GS contributed to conception and design of the study. MF, DD, OK and GS performed experiments and analyzed the data. MF wrote the first draft of the manuscript. MF, DD, OK and GS made the figures, contributed to manuscript revision, read, and approved the submitted version.

Conflicts of Interest: The author declares no conflict of interest.

Introduction

Phrenic motor neurons (PhMNs) located in the cervical spinal cord innervate the diaphragm muscle (DIAm) and their axonal discharges are essential for DIAm activation during a variety of ventilatory and non-ventilatory behaviours [1]. The orderly recruitment of DIAm motor units underpins the effective matching of diverse DIAm pressure and endurance requirements to different behaviours [1,2]. Smaller PhMNs with lower capacitance (higher input resistance) and slower axonal conduction velocities are recruited first for ventilation. By contrast, larger PhMNs with higher capacitance (lower input resistance) and faster axonal conduction velocities are recruited later [1,3], generating the greater pressures required for effective straining and expulsive behaviours (eg. defecation, coughing and sneezing) [1,2].

Smaller PhMNs innervate type I or IIa DIAm fibres comprising Slow (S) or Fatigue-Resistant (FR) motor units, respectively, whilst larger PhMNs innervate type IIx/IIb DIAm fibres comprising Fast Fatigable (FF) motor units [1,2]. During development and throughout the lifespan, the efficacy of DIAm straining and expulsive behaviours is influenced by the abundance and function of FF motor units [1]. In a variety of motor pools FF motor units and their larger constituent motor neurons (MNs) are most vulnerable to degeneration and death in MN conditions such as amyotrophic lateral sclerosis [ALS] [4–8] and ageing [9,10].

Neurotrophic signalling, influences MN function and survival during development [11–15] and various neuromotor disorders [16–21]. There is also evidence that BDNF signalling impacts the maintenance of IIx/IIb fibres of type FF motor units [22]. In particular, brain derived neurotrophic factor (BDNF) via its high-affinity full-length tropomyosin-related kinase ($TrkB_{FL}$) receptor mediates synaptic activity at central and peripheral synapses [14,23], including PhMNs and DIAm [24,25], via mechanisms including the phosphorylation of the transcription factor CREB (pCREB) [26,27] in conjunction with phosphorylated ATF-1 (pATF-1) [28]. When pCREB/pATF-1 is inhibited, neuronal death can ensue [29]. BDNF also signals through truncated ($TrkB_{T1}$ and $TrkB_{T2}$) receptors and the low affinity p75 neurotrophin receptor (p75NTR), all of which have been implicated in MN loss [18,30]. During development, deletion of the $TrkB_{FL}$ receptor causes MN death and perinatal death, precluding the assessment of adults [12]. Using an alternative Cre-Lox approaches, cortical pyramidal neurons undergo morphological remodeling and neuronal death in response to an inducible TrkB deletion (of all TrkB isoforms) in adult mice [31]. Loss and atrophy of MNs within the facial nucleus occurs when $TrkB_{T1}$ is overexpressed following stereotaxic injection of the viral vector promotor [17]. However, the specific effects of impaired $TrkB_{FL}$ signalling on MNs of otherwise healthy animals remains elusive.

We previously found that TrkB inhibition in adult *TrkB*^{F616A} mice impairs DIAm function [32,33]. The *TrkB*^{F616A} chemogenetic mice expresses knock-in alleles that permit rapid, selective and reversible inhibition of $TrkB_{FL}$ kinase activity upon exposure to the kinase inhibitor, 1NMPP1 [34]. To date, MN survival and morphology have not been investigated under conditions of inducible $TrkB_{FL}$ inhibition. As non-invasive intrapleural cholera toxin β labeling of PhMNs is capricious in mice [35], we developed this novel chemogenetic *TrkB*^{F616} rat, with similar DIAm neurotransmission impairments to those of *TrkB*^{F616A} mice [36] to unambiguously assess PhMNs.

We aimed to investigate the effects of inhibited TrkB kinase activity on PhMN survival and morphology. We hypothesized that in *TrkB*^{F616} rats, 1NMPP1-induced inhibition of TrkB kinase will result in PhMN loss and reduced size. We further hypothesized that TrkB kinase inhibition using 1NMPP1 would blunt pCREB/pATF-1 in response to BDNF.

Results

14-day TrkB kinase inhibition does not affect body mass

The initial and final body weights of TrKB kinase inhibited (1NMPP1) and vehicle treated rats were comparable, when sex differences were considered. The final body mass of females in both 1NMPP1 (~259 g, 7.5% increase) and vehicle (~272 g, 5.4% increase) treated groups was significantly lower than males (1NMPP1 ~556 g, 3.7% increase and vehicle ~587 g, 3% increase; $F_{(1,10)}$=4.9, P=0.04, Two-way ANOVA).

14-day TrkB kinase inhibition reduces the number of PhMNs

The rat treatment and PhMN labeling protocol, used to determine the total number of PhMNs and to assess reduced retrograde axonal uptake/transport in the presence of impaired BDNF/TrkB signalling is outlined in Figure 1. In both vehicle and 1NMPP1 rats, we observed robust Alexa-Fluor647 labeling of PhMNs (Figure 2A). In 1NMPP1 rats (207 ± 13), the total numbers of PhMNs were reduced by ~16% compared to vehicle treated rats (245 ± 14; P=0.001, Student's unpaired t-test; Figure 2B).

14-day TrkB kinase inactivity reduces PhMN somal surface area and motor unit size distribution

Based on an unbiased (stereologically determined) sample (Figure 1) of PhMNs (~45 PhMNs per animal; Figure 3), we observed that the mean PhMN somal surface area of PhMNs in 1NMPP1 rats (2096 ± 192 μm^2) was ~25% smaller compared to vehicle treated controls (2768 ± 310 μm^2; P=0.0027, Student's unpaired t-test; Figure 3B).

The distribution of PhMN somal surface areas in 1NMPP1 rats was shifted toward smaller PhMNs compared to vehicle treated controls (P<0.0001, Kolmogorov-Smirnov; Figure 3C).

In a manner identical to prior reports [9,35], PhMNs were binned into size tertiles, based on mean tertile boundaries in vehicle control rats. The % of PhMNs within each tertile was dependent on the interaction between treatment group and size ($F_{(2,24)}$=17.9, P<0.0001, two-way ANOVA), with an increased % of total PhMNs in the smaller size tertile (vehicle: 31%; 1NMPP1: 48%, P=0.0006), unchanged in the medial size tertile (vehicle: 33%; 1NMPP1: 40%, P=0.32), and a decreased % of PhMNs in the larger size tertile (vehicle: 36%; 1NMPP1: 12%, P<0.0001) of 1NMPP1 treated 1NMPP1 rats compared to vehicle controls (Figure 4A).

A similar pattern was found when comparing the absolute numbers of PhMNs within each size tertile, with numbers dependent on the interaction between treatment group and size ($F_{(2,24)}$=16.1, P<0.0001, two-way ANOVA; Figure 4B). In 1NMPP1 rats, there was an 32% greater number of smaller PhMNs (99 ± 12) compared to vehicle controls (74 ± 13; P=0.039; Figure 4B). In 1NMPP1 rats, there was an unchanged number of medial PhMNs

(85 ± 21) compared to vehicle controls (82 ± 23; P>0.99; Figure 5B). In 1NMPP1 rats, there was an 70% reduction in number of larger PhMNs (26 ± 11) compared to vehicle controls (88 ± 17; P<0.0001; Figure 4B).

14-day TrkB kinase inhibition reduces the efficacy of retrograde axonal uptake/transport of CTB in PhMNs

As shown in Figure 5, 14-day TrkB kinase inhibition significantly reduced the number of dual labeled PhMNs. The % of PhMNs labeled only with Alexa Fluor647 CTB is indicative of the failed axonal uptake/transport following 1NMPP1 treatment. The % of PhMNs solely labeled by Alexa Fluor647 CTB was increased ~2.5-fold in 1NMPP1 rats (15 ± 3 %) compared to vehicle rats (6 ± 2 %; P=0.0002, Student's unpaired t-test; Figure 5B).

In 1NMPP1 rats, the somal surface areas of PhMNs solely labeled by Alexa Fluor647 CTB (2626 ± 389 μm^2) was ~33% larger than dual labeled PhMNs (1970 ± 233 μm^2; P=0.0008; Student's Paired t-test; Figure 5C).

TrkB kinase inactivity reduces the number of PhMN dendritic trees

We next investigated the number of primary dendrites emanating from each PhMN soma (Figure 6). The number of primary dendritic trees in rats with 14-day TrkB kinase inactivity (5.3 ± 0.6) was reduced by 24% compared to vehicle controls (7.0 ± 0.5; P=0.0002, Student's unpaired t-test; Figure 6B).

When stratified into tertiles, the number of PhMN primary dendrites was dependent on treatment ($F_{(1,12)}$=29.1, P=0.002; two-way ANOVA). Bonferroni *post hoc* tests revealed a reduced number of PhMN primary dendrites in 1NMPP1 rats, with an ~19% reduction in the smaller tertile (P=0.04), an ~19% reduction in the medial tertile (P=0.016) and an ~29% reduction in the larger tertile (P=0.0001; Figure 6C), compared with vehicle controls.

TrkB kinase inactivity reduces the surface area of the PhMN dendritic arbour

The dendritic arbour of a PhMN comprises the sum surface area or length of each dendritic tree emanating from the soma. We estimated total dendritic arbour surface area by summing the estimated dendritic tree surface areas, using a quadratic approximation previously validated in lumbar MNs [37] and adapted to PhMNs [38], and summing the total for each PhMN assessed. Overall, the total dendritic arbour surface area of 1NMPP1 rats (17140 ± 2195 μm^2) was reduced by ~38% compared to vehicle controls (27690 ± 2733 μm^2; P<0.0001, Student's unpaired t-test; Figure 7A).

When stratified into tertiles, total dendritic arbour surface areas were progressively larger in with the increasing size of the PhMN somal tertile, regardless of treatment group ($F_{(2,24)}$=7.7, P=0.0026; two-way ANOVA; Figure 7B). Total dendritic arbour surface area was also dependent on treatment group ($F_{(1,12)}$=32.1, P=0.0001; two-way ANOVA). Bonferroni *post hoc* tests revealed a reduced dendritic arbour surface area in 1NMPP1 rats, with an ~33% reduction in the medial tertile (P=0.02) and an ~36% reduction in the larger tertile (P=0.0006; Figure 7B), compared with vehicle controls.

Acute TrkB kinase inhibition reduces the abundance of pCREB (serine 133), pATF-1 the pCREB to total CREB ratio and total CREB expression in response to intrathecal BDNF within the cervical spinal cord ventral horn

We have previously shown in the rat that CREB expression increases in response to intrathecal BDNF [39]. As $TrkB_{FL}$ signals through pCREB/pATF-1 [27,40], we assessed the expression of pCREB, pATF-1, total CREB and the pCREB to CREB ratios in *TrkB*^{F616} rats following intrathecal BDNF in vehicle (artificial cerebrospinal fluid) and 1NMPP1-treated rats (Figure 8A). pCREB levels (normalised to total protein) were decreased by ~70% in the BDNF+1NMPP1 group (0.045 ± 0.039, n=4) compared to the BDNF group (0.150 ± 0.103, n=4; P=0.024, Student's unpaired t-test; Figure 8B). pATF-1 levels (normalised to total protein) were decreased almost totally, ~99% in the BDNF+1NMPP1 group (0.0005 ± 0.0002, n=4) compared to the BDNF group (0.0743 ± 0.0303, n=4; P=0.0286, Mann-Whitney U-test; Figure 8C). pCREB/total CREB ratio was decreased by ~32% in the BDNF+1NMPP1 group (0.67 ± 0.14, n=4) compared to the BDNF group (0.46 ± 0.13, n=4; P=0.014, Student's unpaired t-test; Figure 8D). Total CREB (normalised to total protein) was also reduced by ~57% in the BDNF+1NMPP1 group (0.094 ± 0.067, n=4) compared to the BDNF group (0.218 ± 0.109, n=4; P=0.024, Student's unpaired t-test; Figure 8E).

Discussion

The results of the present study demonstrate four main findings in rats with 14-day inhibition of TrkB signalling: i) There is a loss of PhMNs following TrkB kinase inhibition; ii) The distribution of PhMN somal surface area is shifted toward smaller PhMNs following TrkB kinase inhibition; iii) Impaired retrograde axonal uptake/transport is evident in rats with TrkB kinase inhibition, which seems to affect larger neurons; and iv) There is a reduction in the number and size of PhMN dendritic trees following TrkB kinase inhibition. In this study we also demonstrate the potent and rapid inhibition (within one hour) of the main transcription factor associated with reduced TrkB kinase activity – pCREB/pATF-1 in *TrkB*^{F616} rats. Taken together, these results support the hypothesis that BDNF/TrkB signalling has a potent effect on PhMN survival, retrograde axonal uptake/transport and morphology, with a summary of the findings of the present study, and a related investigation of DIAm neuromuscular transmission failure in *TrkB*^{F616} rats [36] presented in Figure 9.

The relationship between increased BDNF/TrkB signalling, maintenance of MN survival is well established during the developmental period of programmed cell death [12] and in response to nerve crush [41]. Frustratingly, BDNF/TrkB signalling becomes more complicated in ageing and adult neuromotor diseases, where different TrkB receptor isoforms (TrkB-truncated) are highly expressed, p75NTR BDNF receptors are more prevalent [17,42,43] and $TrkB_{FL}$ expression declines [44–46]. Indeed, ligand binding to these other receptors (TrkB-truncated and p75NTR) may contribute to MN death, although the precise mechanisms by which this occurs remains obscure, along with age- and disease dependent levels of BDNF bioavailability [18,30]. Adding to this complexity are observations that motor neurons within different neuroanatomical locations within the spinal cord may respond differently to different neurotrophins [47].

In the current study, we were limited in our ability to selectively probe for different TrkB isoforms (including $TrkB_{T1}$ and $TrkB_{T2}$) and p75NTR in PhMNs, as the immunolabelling lacks sufficient specificity [19,48]. In previous evaluations of adult facial motor neurons with viral vectors increasing the expression of $TrkB_{T1}$, concomitant evaluation of $TrkB_{FL}$ was not performed, with the authors speculating that vulnerability was likely dependent on the extent of $TrkB_{T1}$ stifling $TrkB_{FL}$ rather than systematically altering $TrkB_{FL}$ expression [17]. In models of hippocampal excitotoxicity, there is some evidence suggesting that altering levels of $TrkB_{T1}$ does not alter levels of $TrkB_{FL}$ [49], although this is far from conclusive [50].

Regardless, our results indicate an alternative pathway to neuronal death, beyond that of BDNF signalling via $TrkB_{T1}$, $TrkB_{T2}$ and the p75NTR may be occurring. It may be the case that in the smaller MNs that are constantly activated to perform ventilatory behaviours [1], that activity-dependent neurotrophic feedback is sufficient to maintain cellular health via metabolically-sensitive transcription factors (pCREB/pATF-1). By contrast, in the larger PhMNs, seldom activated to perform expulsive airway defence manoeuvres [1], BDNF signalling via $TrKB_{FL}$ is essential to maintain cellular health via the same pCREB/pATF-1 pathway (Figure 9), which when inhibited leads to neuronal death [29]. In support of the non-activity dependent trophic mechanisms being of great importance in FF motor units, BDNF signalling appears to maintain type IIx/IIb muscle fibres [22]. Additionally, axonal transport speeds were identical between S and FR motor axons, yet type FF units alone were non-responsive to BDNF in the SOD1 mouse model of ALS [19]. Future studies uncovering the relative salience of metabolically sensitive transcription factors and altered or alternative BDNF signal transduction via $TrkB_{T1}$, $TrkB_{T2}$ and the p75NTR has critical implications for other neurodegenerative diseases, including those of motor neurons.

In the case of $TrkB_{FL}$ inhibition, germline knockout drastically reduces MN number, although the effect in adults is difficult to study as these knockout rodents do not survive beyond 1–2 days postnatal [12,34]. In adult heterozygote mutants, there is evidence of abundant NMJ morphological disruption and neurotransmission defects are observed [15], although no MN phenotype has been reported. In adult rodents with an inducible $TrkB_{FL}$ knockdown using Cre-lox approaches, neuronal death is readily apparent [31]. In the present study, we had good reason to expect that there would be an effect of TrkB inhibition on PhMN number, as we observed a marked effect of 14-day 1NMPP1 treatment on DIAm neuromuscular transmission [36], consistent with motor unit expansion following PhMN death [36] (Figure 9). Notably, due to the lack of overt denervation at the neuromuscular junction, these impairments are likely due to increased branch point failures due to increased innervation ratios [36] (Figure 9), rather than an effect on release or receptor sensitivity. To determine the effect of impaired TrkB signalling on PhMN survival in adults, we compared PhMN counts in $TrkB^{F616}$ rats treated with 14 days of either Vehicle or 1NMPP1. Thus, we assessed PhMN number and retrograde axonal uptake/transport in $TrkB^{F616}$ rats, where there is no reason to expect that the bioavailability of BDNF is limited. In support of this assumption, intrathecal BDNF did not increase pCREB/pATF-1 in $TrkB^{F616}$ rats acutely treated with 1NMPP1 (this study), nor did BDNF rescue DIAm neuromuscular transmission deficits in $TrkB^{F616}$ rats treated acutely or for 14-days with 1NMPP1 [36], although *ex vivo* approaches have shown altered BDNF levels via ELIZA in DIAm using various stimulation/

blockade approaches [51]. Our approach also obviates the aforementioned problems of differential TrkB expression with age and any negative effects of developmental TrkB deficiency.

Our current findings of ~16% PhMN loss are modest compared to the effects of ageing (~30% bilateral loss of total PhMNs) and unilateral cervical spinal cord contusion injury (~50% loss unilaterally, 25% loss of total bilateral PhMNs) [9,52]. Though mild, the magnitude of difference in PhMN survival is ~triple the variability of our total PhMN counts (CV = ~5 %) (Figure 9). Importantly, there are other major contributions to PhMN loss beyond neurotrophic disturbances in both ageing and unilateral cervical spinal cord contusion injury. The most notable of these is inflammation, with inflammatory cytokines (notably tumour necrosis factor-α) steadily increasing in rodent serum and brain tissue with advancing age [53,54] and is associated with ageing-related MN death [53]. Similar inflammatory cytokine elevations following spinal cord injury may also contribute to MN loss beyond trauma necrosis [55,56]. The interactions between inflammation, oxidative stress, neurotrophins and neuronal death may be more direct than previously assumed, with BDNF/TrkB signalling implicated in mitochondrial homeostasis via TrkB receptors being located on mitochondria [57–59]. However, the direct relationship between dwindled BDNF/TrkB signalling and mitochondrial structure and function within MNs remains unexplored.

The efficacy of BDNF/TrkB signalling itself is dependent on retrograde transport [60–62]. In addition, reduced levels of TrkB have been shown to reduce axonal transport [63], independent of BDNF availability [63]. In neurodegenerative conditions with severe MN loss, such as ALS [4,7,8,64], neurotrophic retrograde signalling is substantially impaired [20,21,43]. In chronic 1NMPP1 rats, we observed a ~two-fold increase in failed retrograde transport of CTB to PhMN somas. The subset of PhMNs that do not take up CTB is present in very low levels in control rats, consistent with past reports comparing “gold-standard” retrograde nerve dip, with ganglioside-dependent [65] CTB retrograde labeling [66]. Importantly, neurons that failed to adequately transport CTB to the soma following chronic inhibition of TrkB kinase were larger than those whose transport remained effective. Thus, TrkB signalling may be more important in PhMNs that are infrequently activated, while those that are continually active may not require substantive neurotrophic support and instead be maintained with activity-related feedback mechanisms (Figure 9). Of great future interest will be the molecular characterization of this subset that fails to adequately engage in retrograde axonal uptake/transport. We speculate that the reinnervation capacity, which is essential throughout the lifespan [67], may be impaired with age in this PhMN population, as indicated by morphological disarray at DIAm NMJs [68–70] and decreased reinnervation capacity observed in old age [71,72].

Other groups have investigated neuronal morphology following BDNF/TrkB signalling inhibition in adults [31]. In MNs, somal size is particularly important, as size serves as the basis for recruitment, as well as for estimating motor unit type differences [1]. Under conditions where MN degenerate (eg. ageing and ALS), larger MNs are more susceptible to death and denervation [4,7,9,10,73–76]. We observed a robust reduction in PhMN somal surface areas of 1NMPP1 rats compared to controls. These findings are similar to those of facial motor neurons following over-expression of $TrkB_{T1}$ [17]. Unlike in ageing, where

the overall range of PhMN size was reduced, without changing the size of the smallest PhMNs [9], a simple death of larger PhMNs does not fully explain our results. Here, our size-distribution analysis shows that chronic TrkB inhibition leads to the shrinking of a discrete fraction of PhMNs in such a manner to have somal surface areas smaller than those of the smallest vehicle controls. There remains the possibility that TrkB inhibition results in a selective loss of larger PhMNs, but our size distributions suggest that remaining PhMNs undergo plastic changes consistent with somal shrinkage. A variety of molecular markers for the motor unit type specification of motor units exist [77–79], with some seemingly more developmental in relevance than true markers of type and most expressing in a gradiated fashion with or without an observed size relationship [7,80,81]. However, their major limitation is the failure to reliably distinguish motor neurons of type FR units from motor neurons of type FF units, hence the apparent loss of size-dependence of motor neuron classification in many of these molecular approaches [7,8,79,82]. The importance of distinguishing FR from FF units is more than just scholarly pedantism, as physiologically, in muscles of mixed motor units, type FR units are recruited to perform a markedly different endurance-related behavioural repertoire (e.g., breathing or walking), compared to the more ballistic activities type FF units are recruited to achieve (e.g., coughing or jumping) [1]. There are also well-documented pathophysiological reasons to evaluate size-dependent loss, with ageing and ALS exhibiting selective vulnerability of FF unit motor neurons and muscle [5–7,9,10,68,76,82–86]. Despite being somewhat arbitrary, the tertile approach to somal sizes allows for a solid physiological basis (i.e., capacitance and recruitment order – see an excellent review [79] for the molecular and functional advantages and limitations to unit type discrimination) for the identification of PhMNs as likely type S and FR or likely type FF.

It has been previously established that the number of dendritic trees and the size of the dendritic arbours are dependent on MN size, with larger MNs having a greater number and size of dendritic trees [5,6,87]. These properties are consistent with passive membrane properties such as capacitance and input resistance determining the order of MN recruitment [1,88]. In other cases of MN loss, the number of dendritic trees and dendritic arbourisations may increase or decrease depending on the motor pool and age of loss [5,6,85,89–91]. In studies where attention was given to MN size, these changes are predominantly in larger MNs, likely due to the increased vulnerability of FF motor units to neuromotor degeneration [5,6,85,87]. In our current study, we show that inhibition of TrkB signalling resulted in reduced surface areas of the entire dendritic post-synaptic domain of PhMNs (i.e., total dendritic surface areas). We interpret this finding as indicative of TrkB signalling being essential to maintain the post-synaptic substrate for PhMN inputs in adult rats. Maintenance of the post-synaptic PhMN domain is likely to be incredibly important in cervical spinal cord injury, where *de novo* inputs to PhMN somas and dendrites are likely to be essential for the recovery of DIAm motor unit function [92–96]. Recovery of DIAm activity has been shown to be dependent on BDNF/TrkB signalling, with gain- and loss-of-function studies cementing the importance of these neurotrophin-associated neuroplasticity mechanisms [24,39,97]. However, despite the abundance of empirical evidence indicating the utility of BDNF/TrkB signalling in DIAm motor unit recovery, the pre- or postsynaptic locus of action, and whether the effect is perisomatic or distal to the PhMN somas is

unknown. Clarifying the effects of TrkB inhibition on PhMN dendrites (size-dependent or otherwise) will prove highly informative for any neurotrophic treatment strategy. Likewise, understanding the influence altered MN somal morphology has on motor unit recruitment and discharge will be valuable in many preclinical contexts.

To date, our studies in the *TrkB*^{F616A} mice and the *TrkB*^{F616} rat have focused on the diaphragm motor unts, evaluating the effects of inhibiting $TrkB_{FL}$ kinase activity on PhMNs (the present study), DIAm NMJs [32,36], DIAm behaviours [33] or the activity of diaphragm motor units following spinal cord injury [97]. However, it is likely that some of the effects of impaired TrkB kinase activity on PhMNs is mediated by supraspinal and spinal neural circuits [1]. These inputs are to PhMNs are myriad [1], with BDNF/TrkB signalling shown to influence brainstem respiratory groups [98] and the pre-Bötzinger complex respiratory pattern generator [99]. Due to the amenability of the rat to robust and detailed functional ventilatory assessments [24,39,52,92,93,96,97], The TrkB^{F616} rat promises to be a useful tool to assess the physiological effects of network-wide TrkB kinase inhibition in sculpting the respiratory rhythm and pattern.

In summary, we provide evidence that inhibition of TrkB signalling in *TrkB*^{F616} rats results in death of PhMNs, reduced retrograde axonal uptake/transport and marked morphological disturbances. We are confident that the *TrkB*^{F616} rat model will be highly useful for examining the effects of TrkB signalling inhibition on PhMN function in various scenarios, particularly ageing and cervical spinal cord injury.

Methods

Animals and anesthesia:

This study was approved by the Institutional Animal Care and Use Committee (IACUC) and all procedures were performed in accordance with American Physiological Society's *Guiding Principles in the Care and Use of Vertebrate Animals in Research and Training*. *TrkB*^{F616} rats were generated on a Sprague Dawley hybrid genetic background and were genetically modified to stably harbor a knock-in mutation in the *Trk* exon (a phenylalanine to alanine substitution) within the kinase subdomain sensitive to PP1 derivatives such as 1NMPP1 [34]. In the presence of 1NMPP1, this mutation results in inhibition of TrkB kinase activity, in a manner similar to the *TrkB*^{F616A} mouse [34] that we have used in previous studies [32]. We chose to develop and use the *TrkB*^{F616} rat model because reliable labeling of the PhMN pool by intrapleural injection of retrograde of CTB is not possible in mice.

All rats were individually housed and maintained on a 12-h light-dark schedule under specific pathogen-free conditions with *ad libitum* access to food and water. For chronic 14-day experiments, adult (4 months of age) female and male *TrkB*^{F616} rats (n=4 per sex, except n=3 per sex in the control group) were used to selectively inhibit TrkB kinase activity following oral 1NMPP1 treatment (25 μM in drinking water). While undergoing chronic 14-day oral 1NMPP1 treatment, water intake was monitored daily. In *TrkB*^{F616A} mice intraperitoneal injections of 1NMPP1 (~0.66 mg/kg) have been shown to inhibit TrkB activity within an hour [33]. Based on the consumption in drinking water (25 μM), ~1.4

mg/kg/day of 1NMPP1 is consumed by *TrkB*^{F616A} mice, similar to the 1.7 mg/kg/day consumed in the present study by our *TrB*^{F616} rats. The dosage in drinking water (25 μM) has previously been shown to be effective at reducing the ratio of phosphorylated TrkB protein to total TrkB protein in protein by ~13-fold in the neural tissue of *TrkB*^{F616A} mice [32]. Treatment duration was based on previous demonstration of substantial DIAm NMTF following 14 days of altered synaptic activity in *TrkB*^{F616} rats [36]. As the rats are drinking water throughout the day, we did not need to determine the half-life of 1NMPP1.

For chronic 14-day experiments, two age-, weight-, and sex-matched groups were studied; DMSO (0.3%; vehicle) treated control *TrkB*^{F616} rats (vehicle; n=7) and 1NMPP1 (25 mM) treated *TrkB*^{F616} rats (TrkB kinase inhibited - 1NMPP1; n=8). For chronic experiments, treatment was initiated when the rats were 4 months of age (initial body weights – ~241 g females and ~536 g males) and continued for 14 days (Figure 1). Treatment duration was based on previous demonstration of substantial DIAm NMTF following 7–14 days of altered synaptic activity in *TrkB*^{F616A} mice [32,33,97] and *TrkB*^{F616} rats [36]. At the terminal experiment, animals were deeply anesthetized by intraperitoneal injection of ketamine (90 mg/kg) and xylazine (10 mg/kg) and then exsanguinated.

To assess the selectivity of the effects of 1NMPP1-induced inhibition on TrkB kinase inhibition following BDNF challenge, we used a second cohort of 8 *TrkB*^{F616} rats. In this experiment, each *TrkB*^{F616} rat, anesthetized by intraperitoneal injection of ketamine (90 mg/kg) and xylazine (10 mg/kg), had a dorsal laminectomy at C_4, followed by an opening of the dura surrounding the spinal cord. Subsequently, we intrathecally infused 40 μL of artificial cerebrospinal fluid with DMSO (the BDNF control group, n=4) or artificial cerebrospinal fluid with 1NMPP1 (25 μM, the BDNF + 1NMPP1 group, n=4) at ~2 μL/min. for 20 minutes. twenty minutes later, 40 μL of BDNF (100 ng/ml; rhBDNF, R&D Systems, Minneapolis, MN) was delivered intrathecally to C_4, at a rate of ~2 μL/min. for 20 minutes. Twenty minutes post BDNF-infusion, the rats were euthanized via exsanguination and fresh ventral horn between C_2-C_6 snap-frozen in liquid nitrogen before being processed for Western blotting.

Labeling PhMNs:

Three days prior to the commencement of DMSO (vehicle) or 1NMPP1 treatment, all rats were intrapleurally injected with Alexa-Fluor647 conjugated CTB (C34778, Thermo Fisher), with CTB previously shown to reliably label all PhMNs in rats [66]. The 3-day period allowed for adequate retrograde transport to all PhMNs prior to any treatment inhibiting TrkB signalling (Figure 1). Three days prior to terminal procedures (i.e., day 11 of treatment), all rats were intrapleurally injected with Alexa-Fluor 488 conjugated CTB (C22841, Thermo Fisher) (Figure 1).

At day 14, following anaesthesia, all rats were euthanized by transcardial exsanguination and perfused with heparinized saline before perfusion with 4% paraformaldehyde (PFA) in 0.1M phosphate-buffered saline (PBS, pH 7.4). The fixed cervical spinal cord was then excised, post-fixed in 4% PFA in PBS overnight, then immersed overnight in 25% sucrose in PBS, prior to cutting 70 μm longitudinal (horizontal) cryostat sections. Sections were

placed on gelatin-coated slides and cover-slipped with DPX mounting media (Fluka, Sigma-Aldritch, St Louis, MO).

Imaging PhMNs for counting and somal size assessment:

Labeled PhMNs in the cervical spinal cord sections were visualized with an Olympus FV2000 laser confocal microscope (Olympus Life Sciences Solutions, Waltham, MA) equipped with argon (488 nm) and green HeNe (640 nm) lasers. Three-dimensional confocal imaging techniques of labeled PhMNs have been previously reported in detail [9,100]. Briefly, all images were acquired at 12-bit resolution in an array of 1024 × 1024 pixels using a 40x Plan Apo oil-immersion objective (NA 1.30) with a step size of 1.0 μm. Sequential two-channel imaging was performed using a dichroic mirror beam splitter that allows transmission of 555–615 nm (reflects 480–555 and 615–800 nm) and appropriate band pass emission filters (495–535 nm and 640–670 nm - for Alexa-Fluor 488 and 647, respectively). To reduce crosstalk, laser illumination was done sequentially for the imaging of each optical slice.

Following imaging, the number of labeled PhMNs was counted on the right side of the spinal cord, noting which PhMNs were dual labeled or labeled with Alexa-Fluor647 or Alexa-Fluor488. The total number of PhMNs, and the somal and dendritic properties of PhMNs was based on assessment of Alexa-Fluor647 (pre-treatment) labelled PhMNs. Within each PhMN pool, the somal surface area of every 5^{th} PhMN was assessed in a stereological manner identical to past studies [9,10,35,100] (Figure 1). Defects in axonal transport/uptake were assessed by the percentage of PhMNs positively labelled with pre-treatment CTB (Alexa-Fluor647) but not post-treatment CTB (Alexa-Fluor647). The long and short axis of PhMNs were measured and used to calculate somal surface areas based on approximations of MN somas to prolate spheroids , as used previously to determine size-dependence of a variety of MN properties [5,6,9]. The number of dendritic trees emanating from PhMN somas was also assessed in a subset of PhMNs, as outlined previously [9]. To determine the dendritic surface area of a particular PhMN, we measured the dendritic diameters of at least 5 PhMNs in each size tertile, in a manner similar to previous studies to [9,35]. These measures were used to estimate the total surface area of an individual PhMN dendritic tree, based on a quadratic formula [37] previously adapted for rat PhMNs [38]. All PhMN number and morphometry outcome measures were also assessed based on somal size tertiles of vehicle rats, in a manner outlined previously [5,6,9,35].

Detection and quantification of proteins using Western blot:

The ventral horn tissues were lysed in 1X RIPA Buffer (Cat. No. 9806, Cell Signaling Technology, Danvers, MA) supplemented with a protease inhibitor cocktail (Cat. No. 11836170001, Roche, Millipore Sigma, Burlington, MA 01803, United States) and phosphatase inhibitors (PhosSTOP, Cat. No. 4906845001, Roche, Millipore Sigma, Burlington, MA 01803, United States). Protein concentrations were quantified using a DC (detergent compatible) protein assay that utilizes the principle of the well-documented Lowry-based assay (Bio-Rad, Berkeley, CA). 60–80 mg of total protein from each sample was denatured in 1X Laemmli sample buffer with beta-mercaptoethanol at 100°C for 3 min. After denaturation, the samples were loaded onto stain-free polyacrylamide gel

(Bio-Rad, Berkeley, CA) and run via SDS-PAGE. Total protein content in each lane was visualized, imaged, and analyzed using the ChemiDoc MP Imaging System (Bio-Rad, Berkeley, CA). The proteins from the gel were then transferred to a polyvinylidene difluoride (PVDF) membrane (Bio-Rad, Berkeley, CA) using the Trans-Blot Turbo system (Cat. No. 1704150EDU, Bio-Rad, Berkeley, CA). After transfer, the membranes were blocked using 5% non-fat dry milk to prevent non-specific binding of antibodies followed by overnight incubation with primary antibodies designed to recognize and bind to the protein of interest (Table 1). Horseradish Peroxidase conjugated species-specific secondary antibodies were used to detect the primary antibody targets and amplify the signal for easier detection (1:7500 dilution). Bands were developed by incubating the PVDF membrane in chemiluminescent SuperSignal West Dura Extended Duration Substrate (Cat. No. PIA34075, Thermo Fisher Scientific, Rockford, IL) for 3 min and visualized using the ChemiDoc MP Imaging System. Band intensity was quantified using Image Lab software and normalized to the total protein visualized in each lane. For pCREB^{S133}, pATF-1 and total CREB detection, the same blot was used to avoid gel-to-gel variation. The blot was probed with rabbit monoclonal pCREB^{S133} specific antibody (Table 1) followed by stripping with Restore Western Blot Stripping Buffer (Cat. No. 46428, Thermo Fisher Scientific, Rockford, IL) to remove the pCREB^{S133} specific antibodies, and the stripped blot was reprobed with mouse monoclonal CREB specific antibody for total CREB detection.

Statistical analysis:

The experimental design is outlined with the procedures, groups, endpoints and primary outcome assessments (Figure 1). The number of animals required to detect a biologically relevant difference of 15% in PhMN numbers was determined by power analysis based on previous reports [9]. Statistical analysis was performed using Prism 8 (Graphpad Software, San Diego, CA) with two-way ANOVA and Bonferroni post-tests used to compare experimental groups size tertile. For two-way ANOVAs omnibus F-values for all results are reported in the results section with Bonferroni *post hoc* values for relevant comparisons. Distributions were evaluated using Kolmogorov-Smirnov tests, with continuous data compared between two groups using unpaired Student's *t*-tests. All data were assessed for normality with Shapiro-Wilk tests, with nonparametric assessments (eg. a Mann-Whitney *U*-test in the case of non-gaussian data). *A priori* it was determined that within a particular data set, any data point outside 2 standard deviations from the mean was excluded from further analysis. Significance was set as $*P<0.05$. All data are presented as means ± 95% confidence intervals (CI), unless otherwise stated. Sex was included as a biological variable in our experimental design; however, previously, we showed that there are no sex differences in the various PhMN [9,10,35,100] properties we examined. Accordingly, when sex as a contributing variable was excluded in the ANOVA, data for females and males were combined for subsequent analyses.

Acknowledgements:

We would like to thank Rebecca Macken, Yun-Hua Fang, and Dr. Wen-Zhi Zhan for their assistance in the completion of this project.

Funding:

Supported by a National Institutes of Health grants R01-AG44615.

References

1. Fogarty MJ; Sieck GC Evolution and Functional Differentiation of the Diaphragm Muscle of Mammals. Compr Physiol 2019, 9, 715–766. [PubMed: 30873594]
2. Sieck GC; Fournier M Diaphragm motor unit recruitment during ventilatory and nonventilatory behaviors. J Appl Physiol 1989, 66, 2539–2545. [PubMed: 2745316]
3. Dick TE; Kong FJ; Berger AJ Correlation of recruitment order with axonal conduction velocity for supraspinally driven diaphragmatic motor units. J Neurophysiol 1987, 57, 245–259. [PubMed: 3559674]
4. Kiernan JA; Hudson AJ Changes in sizes of cortical and lower motor neurons in amyotrophic lateral sclerosis. Brain 1991, 114 (Pt 2), 843–853. [PubMed: 2043953]
5. Fogarty MJ; Mu EWH; Lavidis NA; Noakes PG; Bellingham MC Size-dependent dendritic maladaptations of hypoglossal motor neurons in SOD1(G93A) mice. Anat Rec (Hoboken) 2020, doi:10.1002/ar.24542.
6. Fogarty MJ; Mu EWH; Lavidis NA; Noakes PG; Bellingham MC Size-Dependent Vulnerability of Lumbar Motor Neuron Dendritic Degeneration in SOD1(G93A) Mice. Anat Rec (Hoboken) 2020, 303, 1455–1471, doi:10.1002/ar.24255. [PubMed: 31509351]
7. Dukkipati SS; Garrett TL; Elbasiouny SM The vulnerability of spinal motoneurons and soma size plasticity in a mouse model of amyotrophic lateral sclerosis. J Physiol 2018, 596, 1723–1745, doi:10.1113/JP275498. [PubMed: 29502344]
8. Fogarty MJ Driven to Decay: Excitability and Synaptic Abnormalities in Amyotrophic Lateral Sclerosis. Brain Res Bull 2018, 140, 318–333, doi:10.1016/j.brainresbull.2018.05.023. [PubMed: 29870780]
9. Fogarty MJ; Omar TS; Zhan WZ; Mantilla CB; Sieck GC Phrenic Motor Neuron Loss in Aged Rats. J Neurophysiol 2018, 119, 1852–1862, doi:10.1152/jn.00868.2017. [PubMed: 29412773]
10. Fogarty MJ; Sieck GC Aging affects the number and morphological heterogeneity of rat phrenic motor neurons and phrenic motor axons. Physiol Rep 2023.
11. Sendtner M; Schmalbruch H; Stöckli KA; Carroll P; Kreutzberg GW; Thoenen H Ciliary neurotrophic factor prevents degeneration of motor neurons in mouse mutant progressive motor neuronopathy. Nature 1992, 358, 502–504. [PubMed: 1641039]
12. Klein R; Smeyne RJ; Wurst W; Long LK; Auerbach BA; Joyner AL; Barbacid M Targeted disruption of the trkB neurotrophin receptor gene results in nervous system lesions and neonatal death. Cell 1993, 75, 113–122. [PubMed: 8402890]
13. Garcia N; Santafe MM; Tomas M; Lanuza MA; Besalduch N; Tomas J Involvement of brain-derived neurotrophic factor (BDNF) in the functional elimination of synaptic contacts at polyinnervated neuromuscular synapses during development. J Neurosci Res 2010, 88, 1406–1419, doi:10.1002/jnr.22320. [PubMed: 20029969]
14. Carrasco MA; Castro P; Sepulveda FJ; Tapia JC; Gatica K; Davis MI; Aguayo LG Regulation of glycinergic and GABAergic synaptogenesis by brain-derived neurotrophic factor in developing spinal neurons. Neuroscience 2007, 145, 484–494. [PubMed: 17306467]
15. Kulakowski SA; Parker SD; Personius KE Reduced TrkB expression results in precocious age-like changes in neuromuscular structure, neurotransmission, and muscle function. J Appl Physiol 2011, 111, 844–852, doi:japplphysiol.00070.2011 [pii] 10.1152/japplphysiol.00070.2011. [PubMed: 21737823]
16. Rhymes ER; Tosolini AP; Fellows AD; Mahy W; McDonald NQ; Schiavo G Bimodal regulation of axonal transport by the GDNF-RET signalling axis in healthy and diseased motor neurons. Cell Death Dis 2022, 13, 584, doi:10.1038/s41419-022-05031-0. [PubMed: 35798698]
17. De Wit J; Eggers R; Evers R; Castren E; Verhaagen J Long-term adeno-associated viral vector-mediated expression of truncated TrkB in the adult rat facial nucleus results in motor neuron degeneration. J Neurosci 2006, 26, 1516–1530, doi:10.1523/JNEUROSCI.4543-05.2006. [PubMed: 16452675]

18. Pradhan J; Noakes PG; Bellingham MC The Role of Altered BDNF/TrkB Signaling in Amyotrophic Lateral Sclerosis. Front Cell Neurosci 2019, 13, 368, doi:10.3389/fncel.2019.00368. [PubMed: 31456666]
19. Tosolini AP; Sleigh JN; Surana S; Rhymes ER; Cahalan SD; Schiavo G BDNF-dependent modulation of axonal transport is selectively impaired in ALS. Acta Neuropathol Commun 2022, 10, 121, doi:10.1186/s40478-022-01418-4. [PubMed: 35996201]
20. Henriques A; Pitzer C; Schneider A Neurotrophic growth factors for the treatment of amyotrophic lateral sclerosis: where do we stand? Front Neurosci 2010, 4, 32, doi:10.3389/fnins.2010.00032. [PubMed: 20592948]
21. Lambrechts D; Storkebaum E; Morimoto M; Del-Favero J; Desmet F; Marklund SL; Wyns S; Thijs V; Andersson J; van Marion I; et al. VEGF is a modifier of amyotrophic lateral sclerosis in mice and humans and protects motoneurons against ischemic death. Nat Genet 2003, 34, 383–394. [PubMed: 12847526]
22. Delezie J; Weihrauch M; Maier G; Tejero R; Ham DJ; Gill JF; Karrer-Cardel B; Ruegg MA; Tabares L; Handschin C BDNF is a mediator of glycolytic fiber-type specification in mouse skeletal muscle.Proceedings of the National Academy of Sciences of the United States of America 2019, 116, 16111–16120, doi:10.1073/pnas.1900544116. [PubMed: 31320589]
23. Levine ES; Crozier RA; Black IB; Plummer MR Brain-derived neurotrophic factor modulates hippocampal synaptic transmission by increasing N-methyl-D-aspartic acid receptor activity. Proc Natl Acad Sci U S A 1998, 95, 10235–10239, doi:10.1073/pnas.95.17.10235. [PubMed: 9707630]
24. Sieck GC; Gransee HM; Zhan WZ; Mantilla CB Acute intrathecal BDNF enhances functional recovery after cervical spinal cord injury in rats. J Neurophysiol 2021, 125, 2158–2165, doi:10.1152/jn.00146.2021. [PubMed: 33949892]
25. Mantilla CB; Zhan WZ; Sieck GC Neurotrophins improve neuromuscular transmission in the adult rat diaphragm. Muscle Nerve 2004, 29, 381–386. [PubMed: 14981737]
26. Esvald EE; Tuvikene J; Sirp A; Patil S; Bramham CR; Timmusk T CREB Family Transcription Factors Are Major Mediators of BDNF Transcriptional Autoregulation in Cortical Neurons. J Neurosci 2020, 40, 1405–1426, doi:10.1523/JNEUROSCI.0367-19.2019. [PubMed: 31915257]
27. Finkbeiner S; Tavazoie SF; Maloratsky A; Jacobs KM; Harris KM; Greenberg ME CREB: a major mediator of neuronal neurotrophin responses. Neuron 1997, 19, 1031–1047, doi:10.1016/s0896-6273(00)80395-5. [PubMed: 9390517]
28. Hummler E; Cole TJ; Blendy JA; Ganss R; Aguzzi A; Schmid W; Beermann F; Schutz G Targeted Mutation of the Creb Gene - Compensation within the Creb/Atf Family of Transcription Factors. Proceedings of the National Academy of Sciences of the United States of America 1994, 91, 5647–5651, doi:DOI 10.1073/pnas.91.12.5647. [PubMed: 8202542]
29. Riccio A; Ahn S; Davenport CM; Blendy JA; Ginty DD Mediation by a CREB family transcription factor of NGF-dependent survival of sympathetic neurons. Science 1999, 286, 2358–2361, doi:10.1126/science.286.5448.2358. [PubMed: 10600750]
30. Tessarollo L; Yanpallewar S TrkB Truncated Isoform Receptors as Transducers and Determinants of BDNF Functions. Front Neurosci 2022, 16, 847572, doi:10.3389/fnins.2022.847572. [PubMed: 35321093]
31. Xu B; Zang K; Ruff NL; Zhang YA; McConnell SK; Stryker MP; Reichardt LF Cortical degeneration in the absence of neurotrophin signaling: dendritic retraction and neuronal loss after removal of the receptor TrkB. Neuron 2000, 26, 233–245, doi:10.1016/s0896-6273(00)81153-8. [PubMed: 10798407]
32. Mantilla CB; Stowe JM; Sieck DC; Ermilov LG; Greising SM; Zhang C; Shokat KM; Sieck GC TrkB Kinase Activity Maintains Synaptic Function and Structural Integrity at Adult Neuromuscular Junctions. J Appl Physiol 2014, 117, 910–920, doi:10.1152/japplphysiol.01386.2013. [PubMed: 25170066]
33. Pareja-Cajiao M; Gransee HM; Cole NA; Sieck GC; Mantilla CB Inhibition of TrkB kinase activity impairs transdiaphragmatic pressure generation. J Appl Physiol (1985) 2020, 128, 338–344, doi:10.1152/japplphysiol.00564.2019. [PubMed: 31944892]

34. Chen X; Ye H; Kuruvilla R; Ramanan N; Scangos KW; Zhang C; Johnson NM; England PM; Shokat KM; Ginty DD A chemical-genetic approach to studying neurotrophin signaling. Neuron 2005, 46, 13–21. [PubMed: 15820690]
35. Brandenburg JE; Fogarty MJ; Brown AD; Sieck GC Phrenic motor neuron loss in an animal model of early onset hypertonia. J Neurophysiol 2020, 123, 1682–1690, doi:10.1152/jn.00026.2020. [PubMed: 32233911]
36. Fogarty MJ; Khurram OU; Mantilla CB; Sieck GC Brain derived neurotrophic factor/tropomyosin related kinase B signaling impacts diaphragm neuromuscular transmission in a novel rat chemogenetic model. Front Cell Neurosci 2022, 16, 1025463, doi:10.3389/fncel.2022.1025463. [PubMed: 36385943]
37. Burke RE; Marks WB; Ulfhake B A parsimonious description of motoneuron dendritic morphology using computer simulation. J Neurosci 1992, 12, 2403–2416. [PubMed: 1607948]
38. Obregon G; Ermilov LG; Zhan WZ; Sieck GC; Mantilla CB Modeling dendritic arborization based on 3D-reconstructions of adult rat phrenic motoneurons. Revista Ingenieria Biomedica 2009, 3, 47–54.
39. Mantilla CB; Gransee HM; Zhan WZ; Sieck GC Motoneuron BDNF/TrkB signaling enhances functional recovery after cervical spinal cord injury. Exp Neurol 2013, 247C, 101–109, doi:10.1016/j.expneurol.2013.04.002.
40. Watson FL; Heerssen HM; Moheban DB; Lin MZ; Sauvageot CM; Bhattacharyya A; Pomeroy SL; Segal RA Rapid nuclear responses to target-derived neurotrophins require retrograde transport of ligand-receptor complex. Journal of Neuroscience 1999, 19, 7889–7900. [PubMed: 10479691]
41. Kishino A; Ishige Y; Tatsuno T; Nakayama C; Noguchi H BDNF prevents and reverses adult rat motor neuron degeneration and induces axonal outgrowth. Exp Neurol 1997, 144, 273–286, doi:10.1006/exnr.1996.6367. [PubMed: 9168829]
42. Johnson H; Hokfelt T; Ulfhake B Expression of p75(NTR), trkB and trkC in nonmanipulated and axotomized motoneurons of aged rats. Brain Research Molecular Brain Research 1999, 69, 21–34. [PubMed: 10350634]
43. Mutoh T; Sobue G; Hamano T; Kuriyama M; Hirayama M; Yamamoto M; Mitsuma T Decreased phosphorylation levels of TrkB neurotrophin receptor in the spinal cords from patients with amyotrophic lateral sclerosis. Neurochem Res 2000, 25, 239–245, doi:10.1023/a:1007575504321. [PubMed: 10786708]
44. Johnson H; Hokfelt T; Ulfhake B Decreased expression of TrkB and TrkC mRNAs in spinal motoneurons of aged rats. European Journal of Neuroscience 1996, 8, 494–499. [PubMed: 8963440]
45. Schaser AJ; Stang K; Connor NP; Behan M The effect of age and tongue exercise on BDNF and TrkB in the hypoglossal nucleus of rats. Behavioural brain research 2012, 226, 235–241, doi:10.1016/j.bbr.2011.09.027. [PubMed: 21951697]
46. Personius KE; Parker SD TrkB expression at the neuromuscular junction is reduced during aging. Muscle Nerve 2013, 47, 532–538, doi:10.1002/mus.23616. [PubMed: 23180620]
47. Schaller S; Buttigieg D; Alory A; Jacquier A; Barad M; Merchant M; Gentien D; de la Grange P; Haase G Novel combinatorial screening identifies neurotrophic factors for selective classes of motor neurons. Proc Natl Acad Sci U S A 2017, 114, E2486–E2493, doi:10.1073/pnas.1615372114. [PubMed: 28270618]
48. Kovalchuk Y; Hanse E; Kafitz KW; Konnerth A Postsynaptic Induction of BDNF-Mediated Long-Term Potentiation. Science 2002, 295, 1729–1734, doi:10.1126/science.1067766. [PubMed: 11872844]
49. Rudge JS; Mather PE; Pasnikowski EM; Cai N; Corcoran T; Acheson A; Anderson K; Lindsay RM; Wiegand SJ Endogenous BDNF protein is increased in adult rat hippocampus after a kainic acid induced excitotoxic insult but exogenous BDNF is not neuroprotective. Exp Neurol 1998, 149, 398–410, doi:10.1006/exnr.1997.6737. [PubMed: 9500963]
50. Gomes JR; Costa JT; Melo CV; Felizzi F; Monteiro P; Pinto MJ; Inacio AR; Wieloch T; Almeida RD; Graos M; et al. Excitotoxicity Downregulates TrkB.FL Signaling and Upregulates the Neuroprotective Truncated TrkB Receptors in Cultured Hippocampal and Striatal Neurons.

Journal of Neuroscience 2012, 32, 4610–4622, doi:10.1523/Jneurosci.0374-12.2012. [PubMed: 22457507]

51. Hurtado E; Cilleros V; Nadal L; Simo A; Obis T; Garcia N; Santafe MM; Tomas M; Halievski K; Jordan CL; et al. Muscle Contraction Regulates BDNF/TrkB Signaling to Modulate Synaptic Function through Presynaptic cPKC alpha and cPKC beta I. Front Mol Neurosci 2017, 10, doi:ARTN 147 10.3389/fnmol.2017.00147.
52. Rana S; Sieck GC; Mantilla CB Diaphragm electromyographic activity following unilateral midcervical contusion injury in rats. J Neurophysiol 2017, 117, 545–555, doi:10.1152/jn.00727.2016. [PubMed: 27832610]
53. Katharesan V; Lewis MD; Vink R; Johnson IP Disparate Changes in Plasma and Brainstem Cytokine Levels in Adult and Ageing Rats Associated with Age-Related Changes in Facial Motor Neuron Number, Snout Muscle Morphology, and Exploratory Behavior. Front Neurol 2016, 7, 191, doi:10.3389/fneur.2016.00191. [PubMed: 27872607]
54. Foster KD; Conn CA; Kluger MJ Fever, tumor necrosis factor, and interleukin-6 in young, mature, and aged Fischer 344 rats. Am J Physiol 1992, 262, R211–215, doi:10.1152/ajpregu.1992.262.2.R211. [PubMed: 1539727]
55. Kwiecien JM; Dabrowski W; Dabrowska-Bouta B; Sulkowski G; Oakden W; Kwiecien-Delaney CJ; Yaron JR; Zhang L; Schutz L; Marzec-Kotarska B; et al. Prolonged inflammation leads to ongoing damage after spinal cord injury. PloS one 2020, 15, e0226584, doi:10.1371/journal.pone.0226584. [PubMed: 32191733]
56. Popovich PG; Wei P; Stokes BT Cellular inflammatory response after spinal cord injury in Sprague-Dawley and Lewis rats. J Comp Neurol 1997, 377, 443–464, doi:10.1002/(sici)1096-9861(19970120)377:3<443::aidcne10>3.0.co;2-s. [PubMed: 8989657]
57. Markham A; Cameron I; Bains R; Franklin P; Kiss JP; Schwendimann L; Gressens P; Spedding M Brain-derived neurotrophic factor-mediated effects on mitochondrial respiratory coupling and neuroprotection share the same molecular signalling pathways. European Journal of Neuroscience 2012, 35, 366–374, doi:10.1111/j.1460-9568.2011.07965.x. [PubMed: 22288477]
58. Zoratti M; De Marchi U; Gulbins E; Szabo I Novel channels of the inner mitochondrial membrane. Biochimica et Biophysica Acta 2009, 1787, 351–363, doi:10.1016/j.bbabio.2008.11.015. [PubMed: 19111672]
59. Wiedemann FR; Siemen D; Mawrin C; Horn TF; Dietzmann K The neurotrophin receptor TrkB is colocalized to mitochondrial membranes. Int J Biochem Cell Biol 2006, 38, 610–620, doi:10.1016/j.biocel.2005.10.024. [PubMed: 16343976]
60. Zhou B; Cai Q; Xie Y; Sheng ZH Snapin recruits dynein to BDNF-TrkB signaling endosomes for retrograde axonal transport and is essential for dendrite growth of cortical neurons. Cell Rep 2012, 2, 42–51, doi:10.1016/j.celrep.2012.06.010. [PubMed: 22840395]
61. Ito K; Enomoto H Retrograde transport of neurotrophic factor signaling: implications in neuronal development and pathogenesis. J Biochem 2016, 160, 77–85, doi:10.1093/jb/mvw037. [PubMed: 27318359]
62. Vermehren-Schmaedick A; Olah MJ; Ramunno-Johnson D; Lidke KA; Cohen MS; Vu TQ Molecular-Scale Dynamics of Long Range Retrograde Brain-Derived Neurotrophic Factor Transport Shaped by Cellular Spatial Context. Front Neurosci 2022, 16, 835815, doi:10.3389/fnins.2022.835815. [PubMed: 35431786]
63. Wang T; Martin S; Nguyen TH; Harper CB; Gormal RS; Martinez-Marmol R; Karunanithi S; Coulson EJ; Glass NR; Cooper-White JJ; et al. Flux of signalling endosomes undergoing axonal retrograde transport is encoded by presynaptic activity and TrkB (vol 7, 12976, 2016). Nat Commun 2016, 7, doi:ARTN 13768 10.1038/ncomms13768.
64. Ngo ST; Baumann F; Ridall PG; Pettitt AN; Henderson RD; Bellingham MC; McCombe PA The relationship between Bayesian motor unit number estimation and histological measurements of motor neurons in wild-type and SOD1(G93A) mice. Clin Neurophysiol 2012, 123, 2080–2091, doi:10.1016/j.clinph.2012.01.028. [PubMed: 22521362]
65. Wolf AA; Jobling MG; Wimer-Mackin S; Ferguson-Maltzman M; Madara JL; Holmes RK; Lencer WI Ganglioside structure dictates signal transduction by cholera toxin and association with caveolae-like membrane domains in polarized epithelia. J Cell Biol 1998, 141, 917–927. [PubMed: 9585411]

66. Mantilla CB; Zhan WZ; Sieck GC Retrograde labeling of phrenic motoneurons by intrapleural injection. J Neurosci Methods 2009, 182, 244–249. [PubMed: 19559048]

67. Larsson L Motor units: remodeling in aged animals. J Gerontol A Biol Sci Med Sci 1995, 50 Spec No, 91–95. [PubMed: 7493226]

68. Fogarty MJ; Gonzalez Porras MA; Mantilla CB; Sieck GC Diaphragm neuromuscular transmission failure in aged rats. J Neurophysiol 2019, 122, 93–104, doi:10.1152/jn.00061.2019. [PubMed: 31042426]

69. Prakash YS; Sieck GC Age-related remodeling of neuromuscular junctions on type-identified diaphragm fibers. Muscle Nerve 1998, 21, 887–895. [PubMed: 9626248]

70. Lee KM; Chand KK; Hammond LA; Lavidis NA; Noakes PG Functional decline at the aging neuromuscular junction is associated with altered laminin-alpha4 expression. Aging (Albany NY) 2017, 9, 880–899, doi:10.18632/aging.101198. [PubMed: 28301326]

71. Aare S; Spendiff S; Vuda M; Elkrief D; Perez A; Wu Q; Mayaki D; Hussain SN; Hettwer S; Hepple RT Failed reinnervation in aging skeletal muscle. Skelet Muscle 2016, 6, 29, doi:10.1186/s13395-016-0101-y. [PubMed: 27588166]

72. Hepple RT When motor unit expansion in ageing muscle fails, atrophy ensues. J Physiol 2018, 596, 1545–1546, doi:10.1113/JP275981. [PubMed: 29532916]

73. Hashizume K; Kanda K; Burke RE Medial gastrocnemius motor nucleus in the rat: age-related changes in the number and size of motoneurons. J Comp Neurol 1988, 269, 425–430. [PubMed: 3372722]

74. Jacob JM Lumbar motor neuron size and number is affected by age in male F344 rats. Mechanisms of ageing and development 1998, 106, 205–216. [PubMed: 9883984]

75. Zhang C; Goto N; Suzuki M; Ke M Age-related reductions in number and size of anterior horn cells at C6 level of the human spinal cord. Okajimas Folia Anat Jpn 1996, 73, 171–177. [PubMed: 8942193]

76. Nijssen J; Comley LH; Hedlund E Motor neuron vulnerability and resistance in amyotrophic lateral sclerosis. Acta Neuropathologica 2017, 133, 863–885, doi:10.1007/s00401-017-1708-8. [PubMed: 28409282]

77. Chakkalakal JV; Nishimune H; Ruas JL; Spiegelman BM; Sanes JR Retrograde influence of muscle fibers on their innervation revealed by a novel marker for slow motoneurons. Development 2010, 137, 3489–3499, doi:dev.053348 [pii] 10.1242/dev.053348. [PubMed: 20843861]

78. Enjin A; Rabe N; Nakanishi ST; Vallstedt A; Gezelius H; Memic F; Lind M; Hjalt T; Tourtellotte WG; Bruder C; et al. Identification of Novel Spinal Cholinergic Genetic Subtypes Disclose Chodl and Pitx2 as Markers for Fast Motor Neurons and Partition Cells. Journal of Comparative Neurology 2010, 518, 2284–2304, doi:10.1002/cne.22332. [PubMed: 20437528]

79. Manuel M; Zytnicki D Molecular and electrophysiological properties of mouse motoneuron and motor unit subtypes. Curr Opin Physiol 2019, 8, doi:10.1016/j.cophys.2018.11.008.

80. Morisaki Y; Niikura M; Watanabe M; Onishi K; Tanabe S; Moriwaki Y; Okuda T; Ohara S; Murayama S; Takao M; et al. Selective Expression of Osteopontin in ALS-resistant Motor Neurons is a Critical Determinant of Late Phase Neurodegeneration Mediated by Matrix Metalloproteinase-9. Sci Rep 2016, 6, doi:ARTN 27354.10.1038/srep27354.

81. Misawa H; Inomata D; Kikuchi M; Maruyama S; Moriwaki Y; Okuda T; Nukina N; Yamanaka T Reappraisal of VAChT-Cre: Preference in slow motor neurons innervating type I or IIa muscle fibers. Genesis 2016, 54, 568–572, doi:10.1002/dvg.22979. [PubMed: 27596971]

82. Fogarty MJ The bigger they are the harder they fall: size-dependent vulnerability of motor neurons in amyotrophic lateral sclerosis. J Physiol 2018, 596, 2471–2472, doi:10.1113/JP276312. [PubMed: 29719046]

83. Hegedus J; Putman CT; Gordon T Time course of preferential motor unit loss in the SOD1 G93A mouse model of amyotrophic lateral sclerosis. Neurobiol Dis 2007, 28, 154–164, doi:10.1016/j.nbd.2007.07.003. [PubMed: 17766128]

84. Hegedus J; Putman CT; Tyreman N; Gordon T Preferential motor unit loss in the SOD1 G93A transgenic mouse model of amyotrophic lateral sclerosis. J Physiol 2008, 586, 3337–3351, doi:10.1113/jphysiol.2007.149286. [PubMed: 18467368]

85. Leroy F; Lamotte d'Incamps B; Imhoff-Manuel RD; Zytnicki D Early intrinsic hyperexcitability does not contribute to motoneuron degeneration in amyotrophic lateral sclerosis. Elife 2014, 3, doi:10.7554/eLife.04046.

86. Khurram OU; Fogarty MJ; Sarrafian TL; Bhatt A; Mantilla CB; Sieck GC Impact of aging on diaphragm muscle function in male and female Fischer 344 rats. Physiol Rep 2018, 6, e13786, doi:10.14814/phy2.13786. [PubMed: 29981218]

87. Ma WY; Vacca-Galloway LL Reduced branching and length of dendrites detected in cervical spinal cord motoneurons of Wobbler mouse, a model for inherited motoneuron disease. J Comp Neurol 1991, 311, 210–222, doi:10.1002/cne.903110204. [PubMed: 1721631]

88. Manuel M; Chardon M; Tysseling V; Heckman CJ Scaling of Motor Output, From Mouse to Humans. Physiology (Bethesda) 2019, 34, 5–13, doi:10.1152/physiol.00021.2018. [PubMed: 30540233]

89. Fogarty MJ; Kanjhan R; Bellingham MC; Noakes PG Glycinergic Neurotransmission: A Potent Regulator of Embryonic Motor Neuron Dendritic Morphology and Synaptic Plasticity. J Neurosci 2016, 36, 80–87, doi:10.1523/JNEUROSCI.1576-15.2016. [PubMed: 26740651]

90. Fogarty MJ; Kanjhan R; Yanagawa Y; Noakes PG; Bellingham MC Alterations in hypoglossal motor neurons due to GAD67 and VGAT deficiency in mice. Exp Neurol 2017, 289, 117–127, doi:10.1016/j.expneurol.2016.12.004. [PubMed: 27956032]

91. Fogarty MJ; Mu EWH; Lavidis NA; Noakes PG; Bellingham MC Motor Areas Show Altered Dendritic Structure in an Amyotrophic Lateral Sclerosis Mouse Model. Front Neurosci 2017, 11, 609, doi:10.3389/fnins.2017.00609. [PubMed: 29163013]

92. Fuller DD; Sandhu MS; Doperalski NJ; Lane MA; White TE; Bishop MD; Reier PJ Graded unilateral cervical spinal cord injury and respiratory motor recovery. Respir Physiol Neurobiol 2009, 165, 245–253. [PubMed: 19150658]

93. Lane MA; Lee KZ; Salazar K; O'Steen BE; Bloom DC; Fuller DD; Reier PJ Respiratory function following bilateral mid-cervical contusion injury in the adult rat. Exp Neurol 2012, 235, 197–210, doi:S0014–4886(11)00332–3 [pii] 10.1016/j.expneurol.2011.09.024. [PubMed: 21963673]

94. Lane MA; White TE; Coutts MA; Jones AL; Sandhu MS; Bloom DC; Bolser DC; Yates BJ; Fuller DD; Reier PJ Cervical prephrenic interneurons in the normal and lesioned spinal cord of the adult rat. J Comp Neurol 2008, 511, 692–709. [PubMed: 18924146]

95. Sandhu MS; Dougherty BJ; Lane MA; Bolser DC; Kirkwood PA; Reier PJ; Fuller DD Respiratory neuroplasticity following high cervical hemisection. Respir Physiol Neurobiol 2009.

96. Fogarty MJ; Zhan W-Z; Simmon VF; Vanderklish PW; Sarraf ST; Sieck GC Novel Regenerative Drug, SPG302 Promotes Functional Recovery of Diaphragm Muscle Activity After Cervical Spinal Cord Injury. J Physiol 2023, In Press.

97. Mantilla CB; Greising SM; Stowe JM; Zhan WZ; Sieck GC TrkB Kinase Activity is Critical for Recovery of Respiratory Function after Cervical Spinal Cord Hemisection. Exp Neurol 2014, 261, 190–195. [PubMed: 24910201]

98. Caravagna C; Soliz J; Seaborn T Brain-derived neurotrophic factor interacts with astrocytes and neurons to control respiration. European Journal of Neuroscience 2013, 38, 3261–3269, doi:10.1111/ejn.12320. [PubMed: 23930598]

99. Thoby-Brisson M; Cauli B; Champagnat J; Fortin G; Katz DM Expression of functional tyrosine kinase B receptors by rhythmically active respiratory neurons in the pre-Botzinger complex of neonatal mice. J Neurosci 2003, 23, 7685–7689, doi:10.1523/JNEUROSCI.23-20-07685.2003. [PubMed: 12930808]

100. Fogarty MJ; Rana S; Mantilla CB; Sieck GC Quantifying mitochondrial volume density in phrenic motor neurons. J Neurosci Methods 2021, 353, 109093, doi:10.1016/j.jneumeth.2021.109093.

Highlights

We use a novel TrkBF616 mutant rat to chemogenetically inhibit BDNF/TrkB signaling in otherwise healthy young adult rats

In retrogradely labeled phrenic motor neurons (PhMNs), BDNF/TrkB inhibition leads to PhMN death and reduced axonal transport.

To our knowledge this is the first direct report of motor neuron loss due solely to reduced BDNF/TrkB signaling in adult rats. Our findings have implications for scenarios where BDNF/TrkB signaling is impaired, such as in ALS and aging.

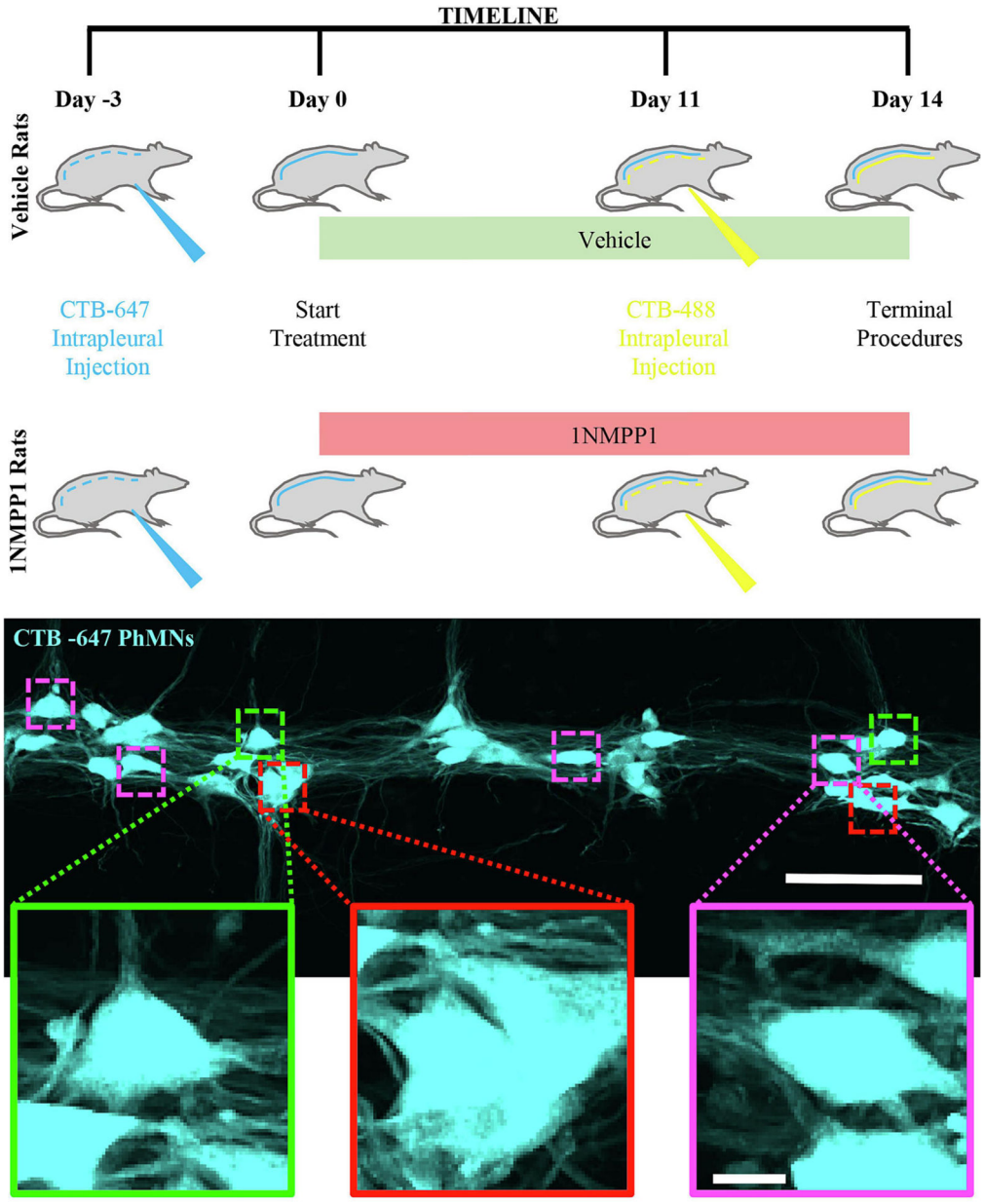

Figure 1: Experimental design, timeline and PhMN sampling.

Timeline shows the order of the experiments, with Vehicle and 1NMPP1 groups randomly separated 3 days prior to the commencement of treatments (day −3) and pre-treatment intrapleural injections of CTB-647 given (dashed blue) to all rats. At day 0, treatment with Vehicle or 1NMPP1 commences. At this time-point CTB-647 has had sufficient time to retrogradely-label PhMNs. At day 11, CTB-488 is intrapleurally injected (dashed yellow) in all rats. By day 14, CTB-488 has had sufficient time to retrogradely-label PhMNs and terminal procedures (transcardial perfusion and tissue excision) are performed. The fluorescent pictomicrograph shows CTB-647 labelled PhMNs within the cervical spinal cord. Our stereological sampling of every 5th PhMN is depicted by the dotted pink frames. In cases where PhMN overlapping creates an ambiguity regarding somal dimensions of the

number of eminating dendritic processes (depicted by dotted red frames), an adjacent PhMN is sampled instead (dotted green frames). Scale bar = 150 μm, inset = 10 μm.

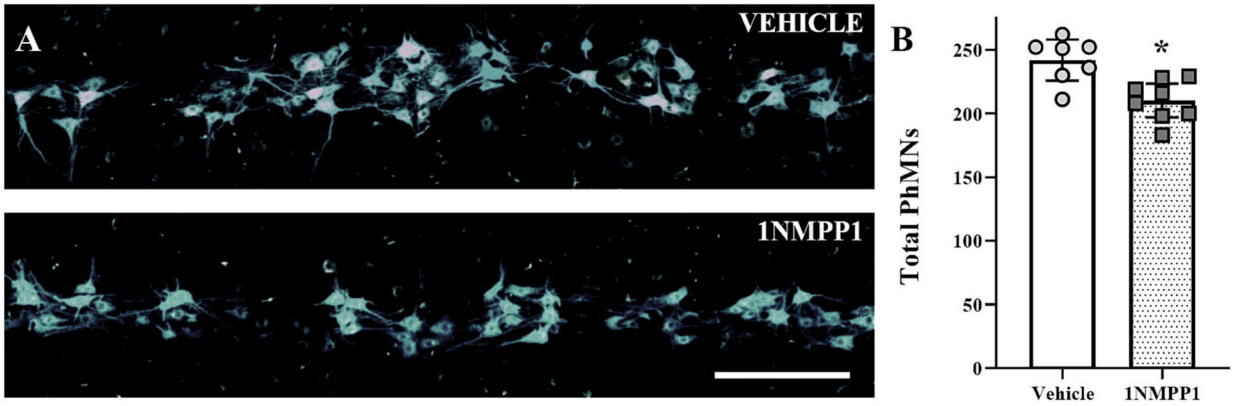

Figure 2: 14-day TrkB kinase inhibition in *TrkB*^{F616} rats reduced PhMN number.

A: Pictomicrographs show PhMNs labeled pre-treatment (blue) with CTB following 14-day Vehicle (top row) or 1NMPP1 treatment (bottom row). **B**: Plot (mean ± 95% CI) shows reduced total PhMNs in 1NMPP1 (dark grey squares) compared to Vehicle rats (light grey circles). Student's unpaired *t*-test, symbols denote a measurement from each rat (*n*), **P*<0.01. Scale bar = 250 μm.

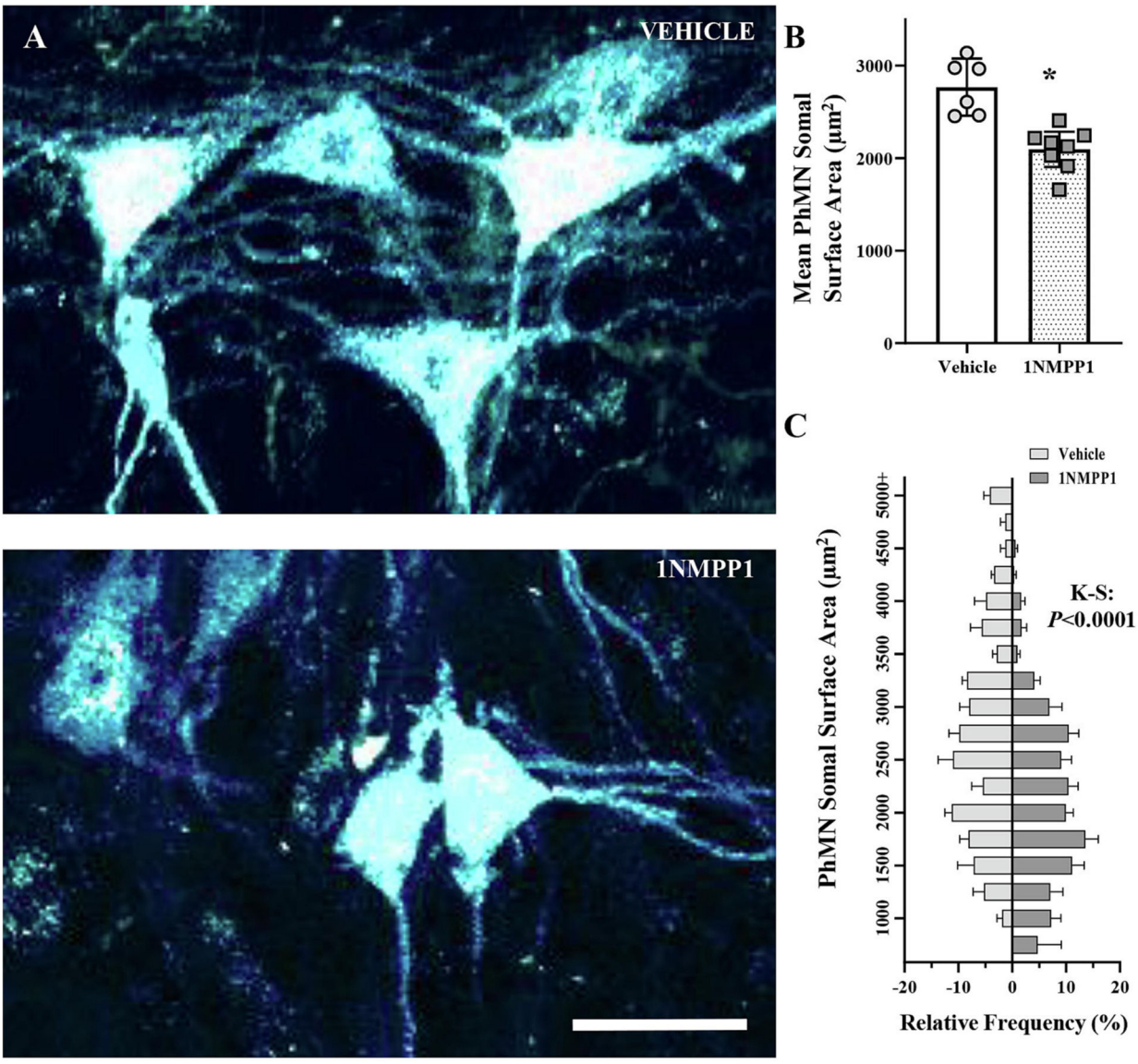

Figure 3: 14-day TrkB kinase inhibition in *TrkB*^{F616} rats reduced somal surface area.

A: High-magnification pictomicrographs show PhMNs labeled pre-treatment (blue) with CTB following 14-day Vehicle (top row) or 1NMPP1 treatment (bottom row). **B:** Plot (mean ± 95% CI) illustrating reduced mean PhMNs somal surface area in 1NMPP1 (dark grey squares) compared to vehicle rats (light grey circles). Student's unpaired *t*-test, symbols denote a measurement from each rat (*n*), **P*<0.05. **C:** Plot (mean ± 95% CI) of relative frequency distribution (%) of PhMNs somal surface area in Vehicle (light grey, left) compared to 1NMPP1 rats (dark grey, right; Kolmogorov-Smirnov, **P*<0.05). Scale bar = 50 μm.

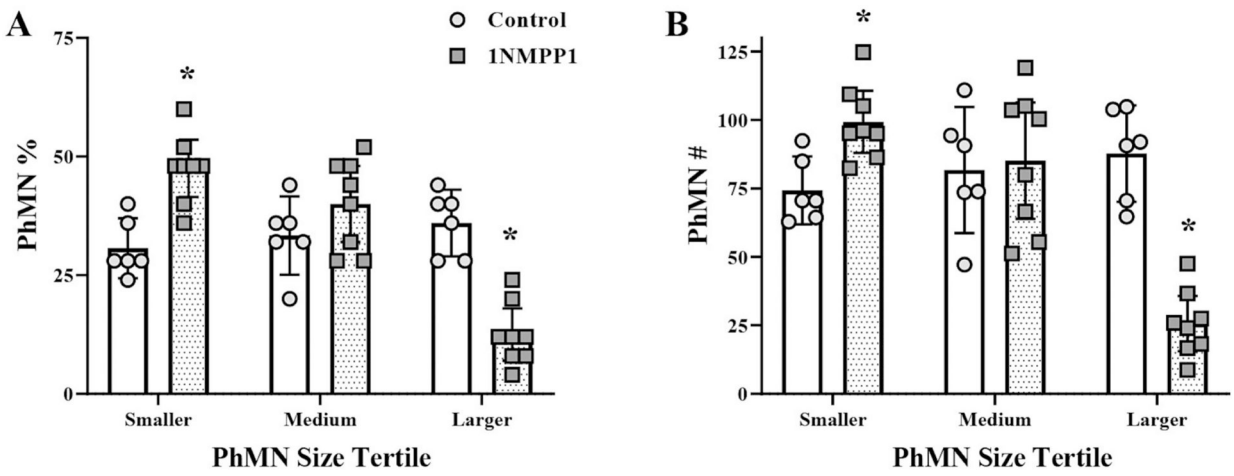

Figure 4: 14-day TrkB kinase inhibition in *TrkB^{F616}* rats alters PhMN somal size tertile populations.

A: As expected, the relative % of PhMNs within each size tertile (mean ± 95% CI) is ~33% in vehicle rats (light grey circles), whereas there is an increased % of smaller PhMNs and a decreased % of larger tertile PhMNs in 1NMPP1 rats (dark grey squares). Two-way ANOVA with Bonferroni *post hoc* test, symbol denotes a data point from an individual rat (*n*), **P*<0.05. **B**: As expected, the number of PhMNs within each size tertile (mean ± 95% CI) is ~80 in vehicle rats (light grey circles), whereas there is an increased number of smaller PhMNs and a decreased number of larger tertile PhMNs in 1NMPP1 rats (dark grey squares). Twoway ANOVA with Bonferroni *post hoc* test, symbol denotes a data point from an individual rat (*n*), **P*<0.05.

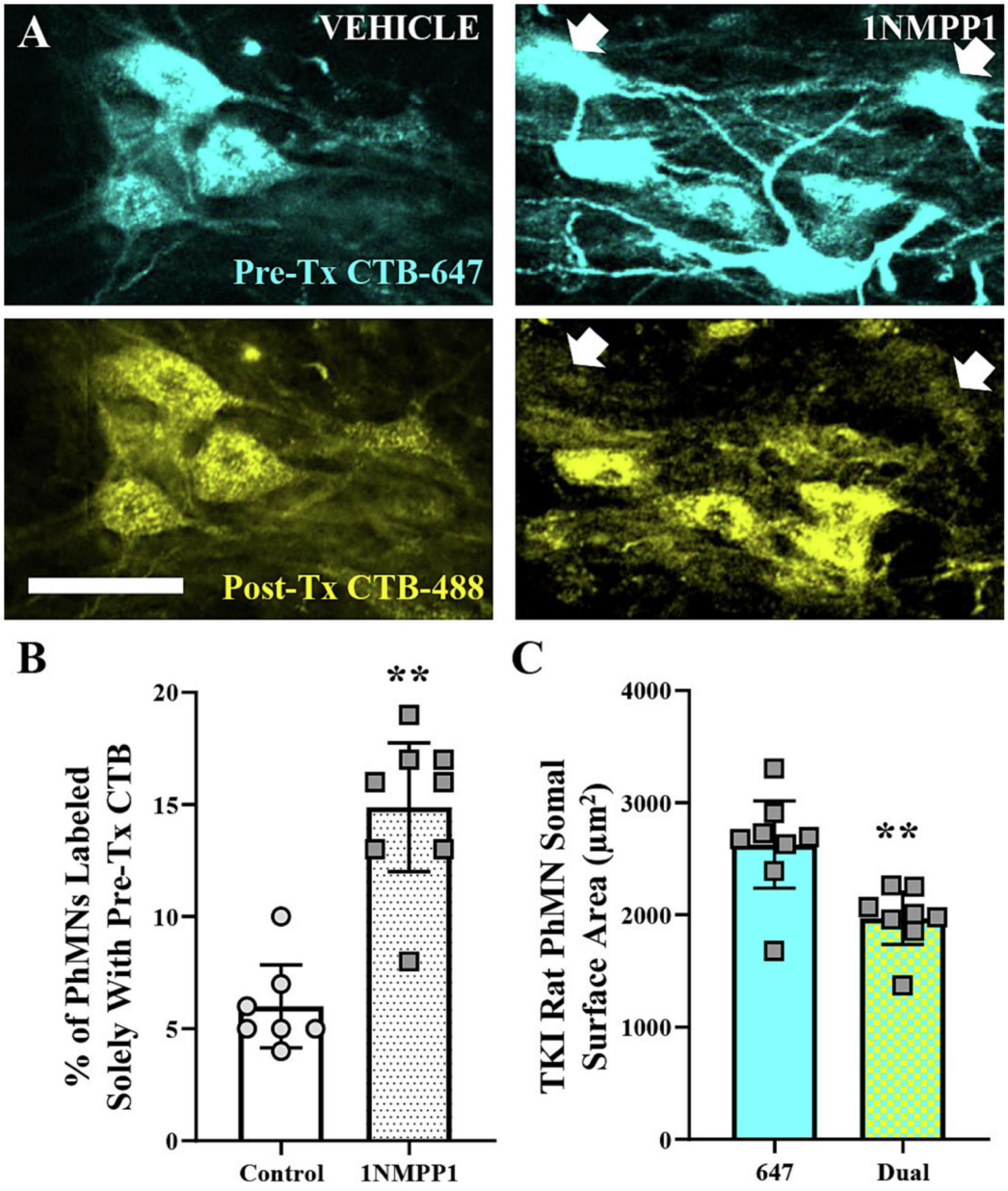

Figure 5: 14-day TrkB kinase inhibition in *TrkB*^{F616} rats reduces retrograde axonal uptake/ transport of CTB.

A: Photomicrographs showing CTB labeled PhMNs before (Pre-Tx CTB - blue) and after (Post-Tx CTB - yellow) treatment with vehicle (VEH, left column) or 1NMPP1 (right column). **B:** Plot (mean ± 95% CI) shows increased % of Pre-Tx CTB labeled PhMNs in 1NMPP1 (dark grey squares) rats (i.e., a failure of retrograde Post-Tx CTB axonal uptake/ transport under conditions of impaired BDNF/TrkB signalling) compared to vehicle controls (light grey circles). Student's unpaired *t*-test, each symbol represents one rat, **P*<0.05. **C:** Plot (mean ± 95% CI) shows decreased PhMN somal surface area of dual-labeled (Pre-Tx CTB and Post-Tx CTB) PhMNs compared to Alexa-Fluor647 Pre-Tx CTB labeled PhMNs in 1NMPP1 (dark grey squares) rats (i.e., the failure of retrograde Post-Tx CTB axonal uptake/transport under conditions of impaired BDNF/TrkB signalling was primarily in larger

PhMNs). Student's paired *t*-test, each symbol represents one rat, **P*<0.05. Scale bar = 50 μm.

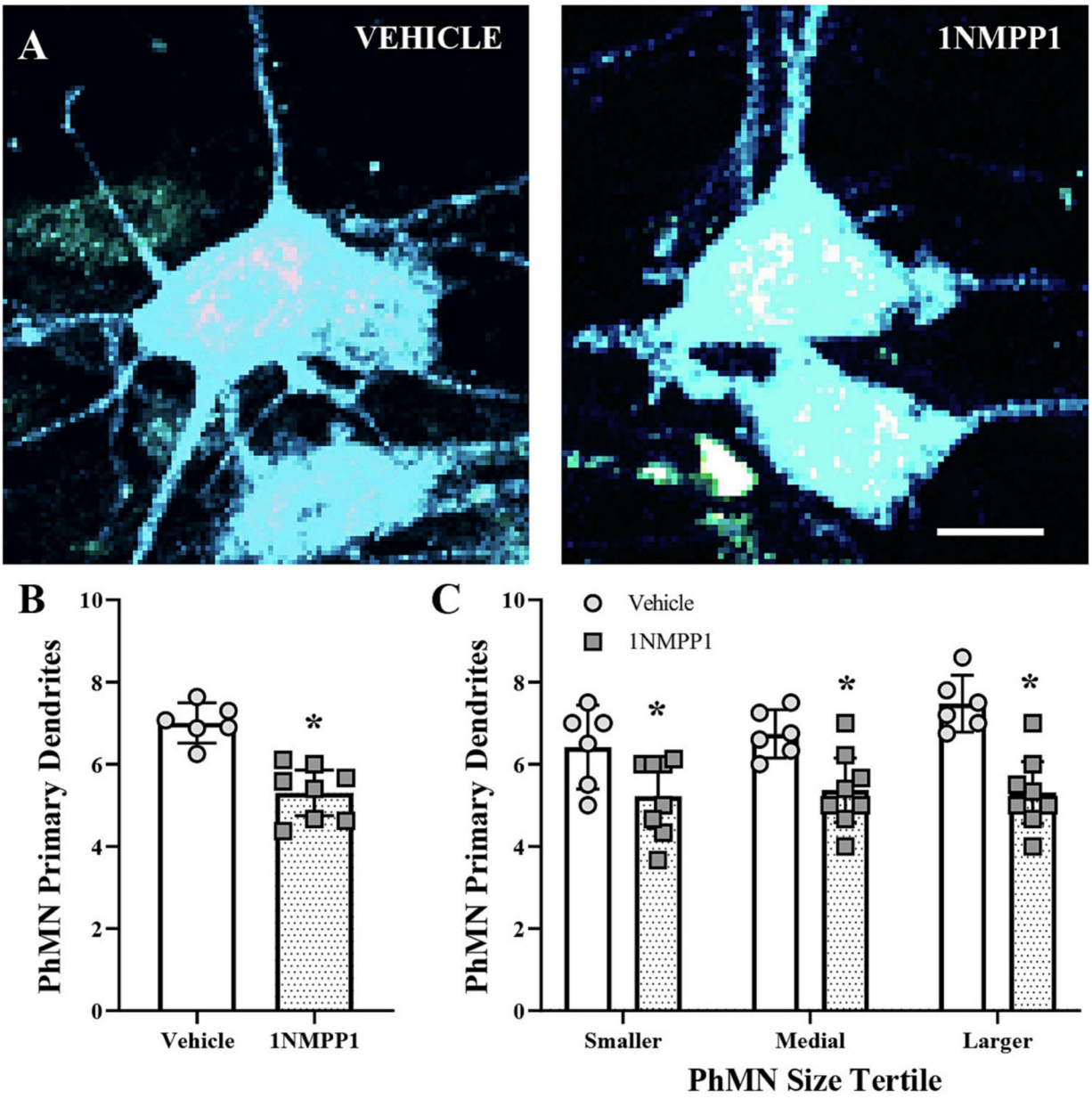

Figure 6: 14-day TrkB kinase inhibition in *TrkB*^{F616} rats reduces the number of PhMN dendritic trees.

A: Photomicrographs showing CTB labeled PhMNs and their proximal dendrites in vehicle (left) and 1NMPP1 (right) rats. **B**: Plot (mean ± 95% CI) shows decreased PhMN primary dendrites (i.e., reduced dendritic trees) in 1NMPP1 (dark grey squares) compared to vehicle (light grey circles) rats. Student's unpaired *t*-test, each symbol represents one rat, **P*<0.05. **C**: Plot (mean ± 95% CI) shows decreased PhMN primary dendrites in 1NMPP1 (dark grey squares) compared to vehicle (light grey circles) rats in smaller, medial and larger PhMN size tertiles. Two-way ANOVA with Bonferroni *post hoc* test, symbol denotes a data point from an individual rat (*n*), **P*<0.05.

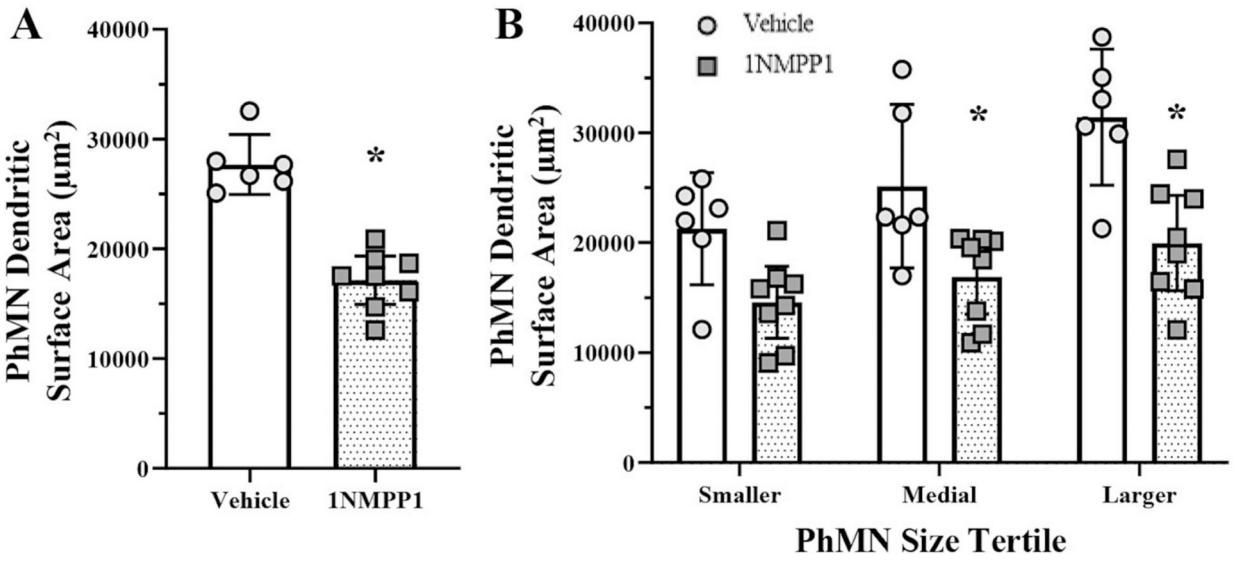

Figure 7: 14-day TrkB kinase inhibition in *TrkB*^{F616} rats reduces the estimated surface area of PhMN dendritic trees.

A: Plot (mean ± 95% CI) shows decreased PhMN dendritic arbour surface area in 1NMPP1 (dark grey squares) compared to vehicle (light grey circles) rats. Student's unpaired *t*-test, each symbol represents one rat, **P*<0.05. **B**: Plot (mean ± 95% CI) shows decreased PhMN dendritic arbour surface area in 1NMPP1 (dark grey squares) compared to vehicle (light grey circles) rats in medial and larger PhMN size tertiles. Two-way ANOVA with Bonferroni *post hoc* test, symbol denotes a data point from an individual rat (*n*), **P*<0.05.

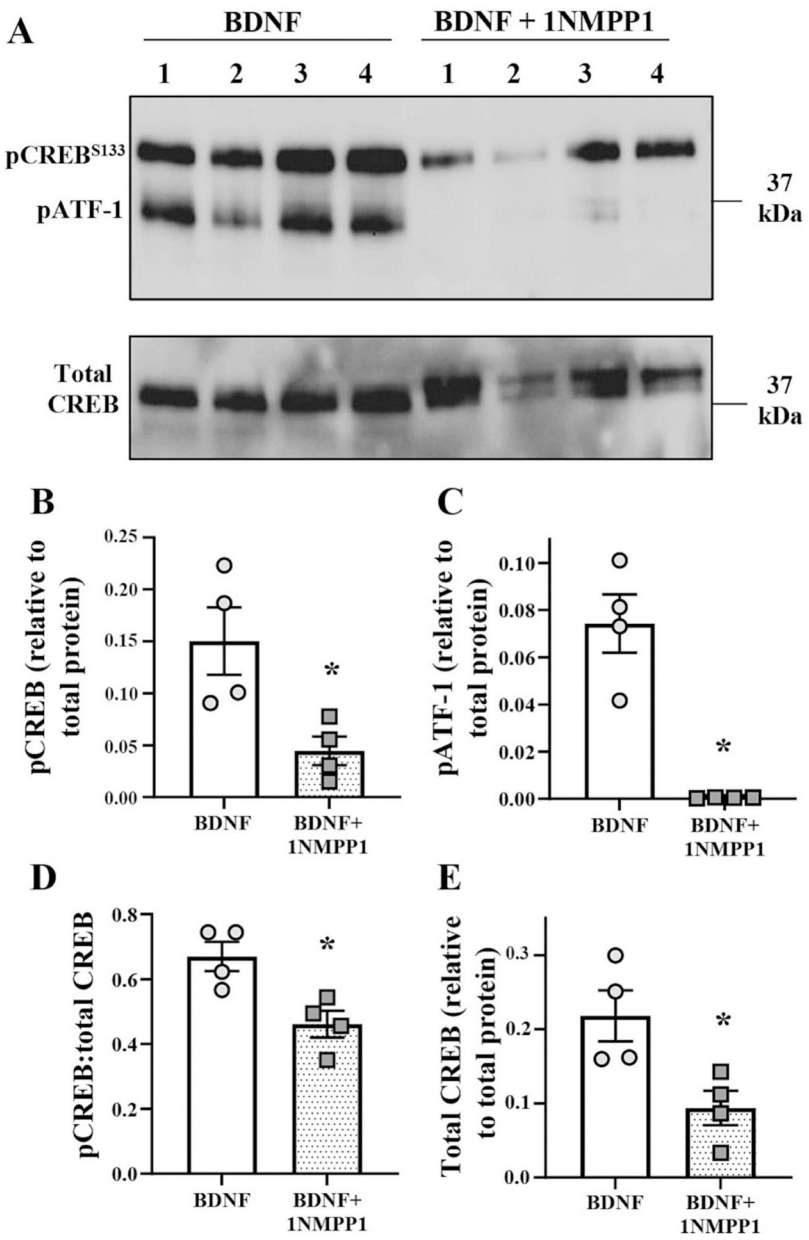

Figure 8: Acute TrkB kinase inhibition in *TrkB^{F616}* rats reduces the pCREB response to intrathecal BDNF in the ventral horn of the cervical spinal cord.

A: Shows Western blot gels of pCREB^{s133,} its alternative pATF1 total CREB in rats acutely exposed to intrathecal BDNF (BDNF group) and rats acutely exposed to BDNF following 1NMPP1 pre-treatment (BDNF+1NMPP1 group). **B**: Plot (mean ± SEM) shows decreased pCREB relative to total protein in BDNF+1NMPP1 (dark grey squares; n=4) compared to BDNF (light grey circles; n=4) rats. Student's unpaired t-test, each symbol represents one rat, *P<0.05. **C**: Plot (mean ± SEM) shows decreased pATF-1 relative to total protein in BDNF+1NMPP1 (dark grey squares; n=4) compared to BDNF (light grey circles; n=4) rats. Student's unpaired t-test, each symbol represents one rat, *P<0.05. **D**: Plot (mean ± SEM) shows decreased pCREB:total CREB ratio in BDNF+1NMPP1 (dark grey squares; n=4) compared to BDNF (light grey circles; n=4) rats. Student's unpaired t-test, each symbol

represents one rat, *P<0.05. **E**: Plot (mean ± SEM) shows decreased total CREB relative to total protein in BDNF+1NMPP1 (dark grey squares; n=4) compared to BDNF (light grey circles; n=4) rats. Student's unpaired t-test, each symbol represents one rat, *P<0.05.

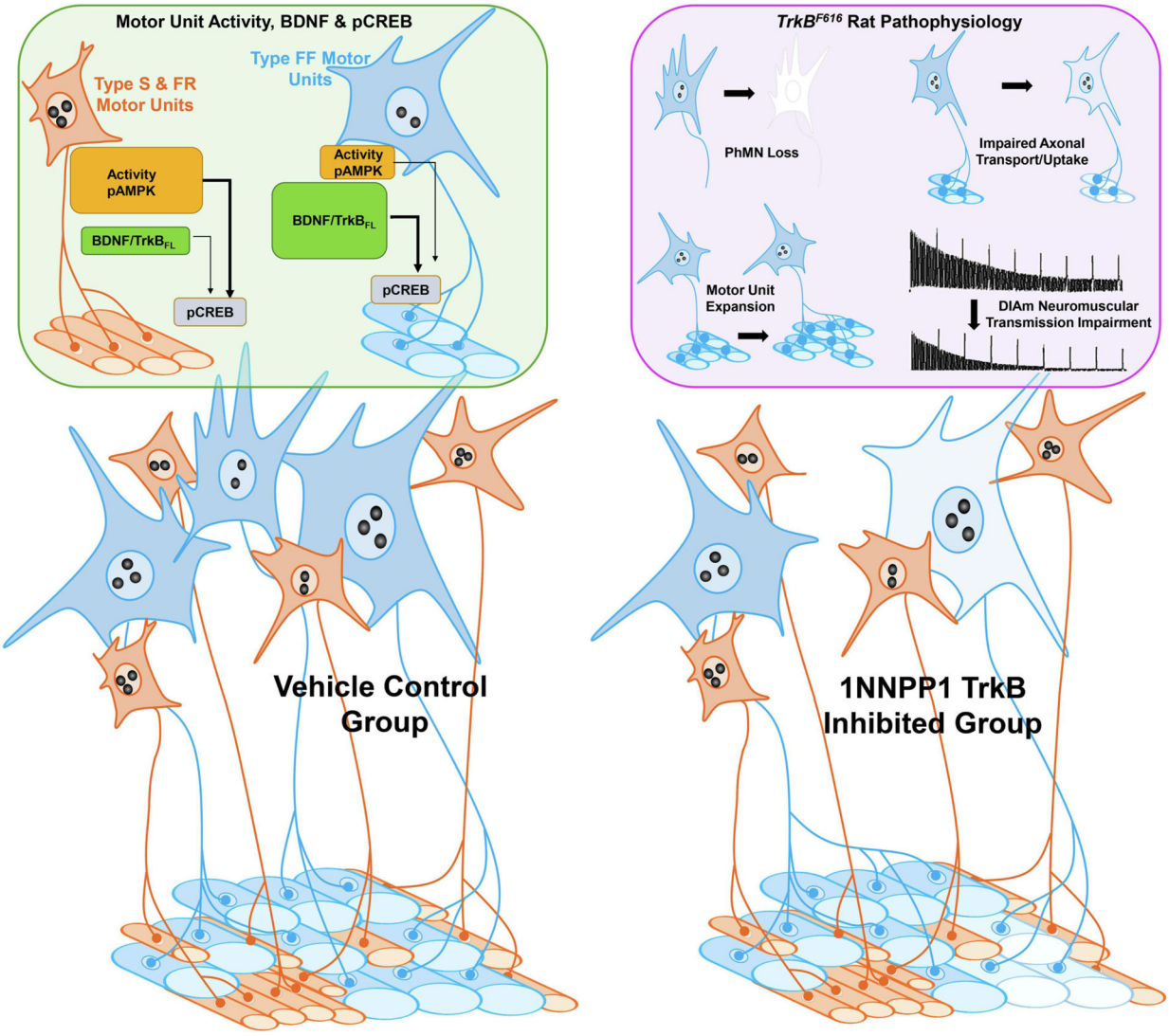

Figure 9: Mechanism for motor unit type differences in BDNF/TrkB neurotrophic support.

Green Box: Both motor unit activity and BDNF/TrkB signalling pathways promote phosphorylation of CREB (pCREB). In type S and FR motor units (orange), this is facilitated by their high degree of activity (incessant recruitment during breathing) and pAMPK leading to sufficient pCREB. In type FF motor units (blue), the relative activity level is lower (recruited only for straining/expulsive manoeuvres) and are thus more dependent on BDNF/TrkB signalling than activity *per se* to maintain sufficient pCREB. **Lavender Box:** The *TrkB*^{F616} rat exhibits a variety of deficits throughout the motor unit. We observe a loss of larger (likely FF) phrenic motor neurons (PhMNs) and consequent motor unit expansion. We have not noted deficits of presynaptic innervation of postsynaptic nerve terminals, yet have observed impaired axonal transport/uptake in larger (likely FF) PhMNs. In addition, we have previously reported impaired neuromuscular transmission in *ex vivo* phrenic nerve diaphragm muscle assessments. **Open Portion:** In the vehicle control group, type S and FR motor units (orange) and type FF motor units are able to achieve the full gamut of ventilatory and non-ventilatory diaphragm muscle behaviours and are supported

via both activity and neurotrophic mechanisms. In the TrkB inhibited group, frank loss of PhMNs, increased innervation ratios and impaired axonal transport/uptake likely contribute to the deficits we observe in DIAm neuromuscular function.

Table 1:

Primary antibodies used for Western blot

Primary Ab	Manufacturer	Catalog Number	Application	Dilution
pCREB^{S133}	Cell Signaling Technology	9198S	Western blot	1:1000
CREB	Cell Signaling Technology	9104S	Western blot	1:1000